



Building up a subsurface geological model in active offshore areas: constraints from legacy seismic reflection profiles and deep wells in the 2022 Fano-Pesaro Mw 5.5 earthquake sequence area (Adriatic Sea, Italy).

5 Elham Safarzadeh¹, Maurizio Ercoli^{1,3}, Filippo Carboni^{2,3}, Francesco Mirabella¹, Assel Akimbekova⁴,
Massimiliano R. Barchi¹

¹Department of Physics and Geology, University of Perugia, Italy

²Institute of Earth and Environmental Sciences (Geology), Albert-Ludwigs-University Freiburg, Germany

10 ³CRUST Member (Centro interUniversitario per l'analisi SismoTettonica Tridimensionale ConApplicazioni Territoriali),
Italy

⁴Eni Exploration and Production Division, Via Emilia, 1, 20097 San Donato Milanese, Milan, Italy

Correspondence to: Safarzadeh, E (elham.safarzadeh@dottarandi.unip.it)

Abstract. Building a geological model in offshore areas is a complex task, due to the obvious absence of outcrops and thus
15 the inaccessibility to the study site. The integration of key seismic reflection and borehole data is therefore fundamental,
even if only available as legacy data on paper hard copy and/or characterized by an apparent low quality. However, such data
are often the only ones available, and can still provide a high amount of detailed information for building a reliable
geological model to compare and discuss with seismicity distribution in active areas. In this work, legacy seismic reflection
profiles calibrated with boreholes are used to propose a new geological model of the frontal part of the Northern Apennines
20 area struck by the 2022 Fano-Pesaro Mw 5.5 earthquake sequence (Adriatic Sea, Italy). The observed tectonic structures are
originated by multiple décollements located at different depths and show a strong relationship between the faulting depth and
the anticlines wavelength. Two structures, namely Pesaro and Cornelia anticlines, are interpreted as related to deep-seated
thrusts, showing an en-echelon arrangement and thin-skinned deformation. A smaller wavelength structure, namely Tamara
antiform, is interpreted to be related to shallow-seated imbricated fore-verging thrusts in the forelimb of the Pesaro anticline.
25 We highlight the importance of constructing a well-constrained geological model by integrating legacy geological and
geophysical data, aimed at offshore seismotectonic studies as well as at industrial applications, particularly in the context of
energy transition.

1. Introduction

Buried and blind thrust faults, particularly those beneath the seafloor, pose considerable difficulties for the study of global
30 seismic activity (Berberian, 1995; Roering et al., 1997; Gunderson et al., 2013; Panara et al., 2021). Despite their hidden



nature, ~~they pose substantial natural hazard being~~ capable to produce strong earthquakes and related underwater landslides, and tsunamis (Lettis et al., 1997; Ioualalen et al., 2017; Takashimizu et al., 2020; Maramai et al., 2022). As coastal populations and infrastructure expand, the understanding of the behaviour of these offshore buried faults becomes essential for mitigating both seismic and tsunami risks. Their detection is especially challenging as it heavily relies on indirect observations such as geophysical data (Roering et al., 1997; Déverchère et al., 2005; Hayes et al., 2010; Sorlien et al., 2013; Franklin et al., 2019). Seismic reflection is one of the best geophysical tools able to provide high-resolution images of the subsurface, being capable of illuminating depths where the upper crust earthquakes are located. These data are suitable to identify the faults geometry, kinematics, hierarchy and dynamics as well as the overall subsurface geological setting and position of the different lithological bodies which possess different velocity of seismic waves propagation (e.g. Chiaraluce et al., 2017).

The Adriatic Sea in central Italy (Fig. 1) is a clear challenging example in terms of risk assessment, as the nearby coastlines are densely populated and many critical infrastructures have been developed during the last tens of years. In this region, the buried and blind thrust faults, present in the offshore area, play a key role in the regional seismotectonic setting, but their detection is particularly challenging due to the high sedimentation rate of the area (Ricci Lucchi, 1986; Frignani and Langone, 1991; Barbieri et al., 2007; Ghielmi et al., 2013; Amadori et al., 2020) and the general low-quality of the available geophysical data, frequently being legacy seismic reflection profiles.

While the axial zone of the Northern Apennines, located about 70 km onshore to the West, is affected by extensional seismicity (Lavecchia et al., 1994; Ciaccio et al., 2005; Chiaraluce et al., 2017; Porreca et al., 2018; Barchi et al., 2021; Sukan et al., 2023), the seismic events recorded in the offshore Marche region are mainly compressive, caused by buried active thrusts faults (Argnani, 1998; Maesano et al., 2013; Brancolini et al., 2019; Panara et al., 2021; Montone & Mariucci, 2023; Maesano et al., 2023; Pezzo et al., 2023, Lavecchia et al., 2023). The related active contraction, affecting the Periadriatic region is testified by historical seismicity (Boschi et al., 2000; Guidoboni et al., 2019; Rovida et al., 2022), and by many observations derived by geodetic (Bigi et al., 1992; D'agostino et al., 2008; Palano et al., 2020; Pezzo et al., 2020), geological, geophysical (Finetti & Del Ben., 2005; Fantoni & Franciosi, 2010; Ghielmi et al., 2010; Tinterri & Lipparini, 2013; Casero and Bigi, 2013) and seismotectonic studies (Di Bucci and Mazzoli, 2002; Maesano et al., 2013; Brancolini et al., 2019; Panara et al., 2021; Montone & Mariucci, 2023; Carboni et al., 2024).

The subsurface offshore thrust faults and related folds in the study area are part of the latest contractional structures associated with the evolution of the Northern Apennines thrust belt. The contractional structures possess similar geometry to that of the outcropping westward structures, where the chain is exposed (e.g. Mazzanti and Trevisan, 1978; Alvarez, 1999; Barchi, 2010). In the Northern Apennines in particular, previous work suggested that at least two main sets of structures, namely the Umbria-Marche folds ("deep-seated - large - structures") and shallow imbricates ("shallow-seated - small - structures") coexist (multiple décollements model - Massoli et al., 2006). These two sets of structures have different characteristics and significance. Weak décollements, located at different depths, influence the geometry and kinematics of the thrust systems. Such décollements largely govern the thrusts dimension and evolution, so that the deeper the décollement,



the larger the wavelength of the structure (Barchi et al., 1998; Barchi et al., 2010). These considerations are supported by both field observations (e.g., Koopman, 1983; De Feyter, 1986) and former seismic interpretation works in the same region (Pieri and Groppi, 1981; Castellarin et al., 1985; Bally et al., 1986; Barchi et al., 1998; Pauselli et al., 2002) and further areas in the Central Adriatic Sea. (e.g., Carboni et al., 2024).

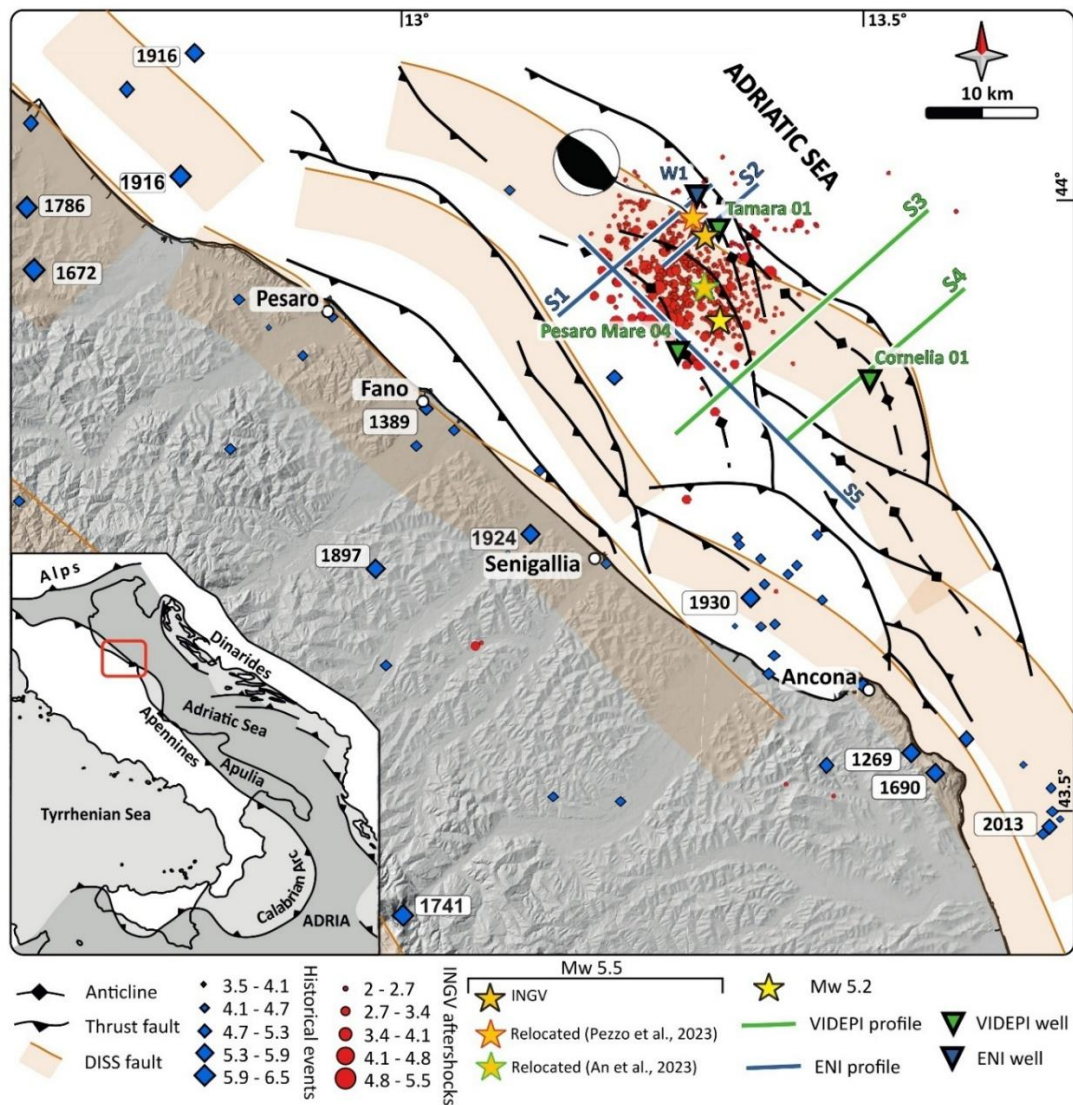


Fig.1. Seismotectonic framework of the Northern Adriatic Sea. Red dots indicate the recorded seismicity from 9th November 2022 until 1st of January 2025, including magnitudes higher than Mw 1.7 (959 events) and the focal mechanism of the main shock (9th November 2022). The orange and yellow stars indicate the main shocks of the 9th November 2022 earthquake events, provided by INGV (INGV). The blue diamond shapes indicate the seismicity of the region derived from both instrumental and non-instrumental archived earthquakes from years 1269 to 2019, obtained from CPTI15-DBMI15v.4.0 (Rovida et al., 2022 and Locati et al., 2022). Seismogenic sources are from DISS 3.3.0 (DISS Working Group, 2021), while the fault traces are from Maesano et al. (2023).



80 The subsurface geological setting of a seismically active area is hence crucial not only for the identification of the active causative fault segment, but also to identify the lithologies involved in seismic faulting (e.g. Mirabella et al., 2008). In addition, the position of the subsurface geological **bodies** also affects **the distribution of the associated different velocity blocks which are fundamental in earthquake location studies** (Latorre et al., 2016).

This study focuses on the recent seismic sequence occurred in the southern portion of the Northern Adriatic (NA) Sea, about 85 25 km offshore from the coastal towns of Fano and **Pesaro** (Fig. 1), which caused damage along the entire coast of the Marche Region. This area experienced significant seismic activity starting from November 2022, culminating with a Mw 5.5 earthquake on the 9th of November 2022. One minute later, a Mw 5.2 earthquake followed the first event, approximately 8 km more to the south-southeast. The **focal mechanisms of both earthquakes indicated almost pure thrust-slip motion along a NW-SE striking fault** (Pezzo et al., 2023). This earthquake sequence, at the end of December 2024, recorded over 560 90 aftershocks larger than Mw 2 (<http://terremoti.ingv.it>).

In this study, an extensive investigation across an area of about 1400 km² of the Adriatic Sea offshore Pesaro and Ancona towns, has been carried out. A comprehensive data analysis has been accomplished across this region, in order to understand and shed light on the geological and structural settings, aiming to provide insights on its tectono-stratigraphic evolution and to its seismotectonic character. Therefore, stratigraphic and geophysical analysis as well as extensive seismic interpretation 95 were carried out on selected wells and legacy reflection seismic profiles, including both unpublished (commercial) and freely available data stored in public databases (<https://www.videpi.com>). This study aims to demonstrate the importance of a thoughtful re-use and revision of such offshore data. **This workflow is mandatory** to build up a reliable geological model to be compared and integrated with seismicity, particularly because no surface outcrops are clearly available, and there exist well-known uncertainties characterizing the offshore earthquakes relocations. **The joint use of seismic reflection profiles,** 100 **calibrated with borehole stratigraphy.**

2. Geological, Structural settings and regional seismicity.

The NA Sea is predominantly composed of continental crust (Ollier & Pain., 2009; Piccardi et al., 2011) and represents the deformed foreland of the surrounding orogenic belts, including the Apenninic belt to the West, the Dinarides-Albanides to the East, and the southern Alps to the North (Fig.1). The Adriatic Sea is composed of different stratigraphic units registering 105 the initial drowning and the subsequent emersion of the Tethys margin (e.g., Finetti & Del Ben., 2005; Casero and Bigi, 2013). The initial rifting phase led to the deposition of Permian–Anisian sandstones interbedded with dolostones, limestones, gypsum and salt. During the Late Triassic, the normal faults accommodating the initial Tethys rifting, allowed the deposition of evaporitic deposits and shallow-water carbonate sequences (Mattavelli et al., 1991, Geletti et al., 2008; Carminati et al., 2013; Wrigley et al., 2015). The further sea opening promoted the growing of extensive carbonate platforms during the 110 Lower Jurassic, which were subsequently buried by the deposition of Lower Jurassic–Palaeocene intraplate pelagic



carbonate succession (e.g., Centamore et al., 1992; Menichetti and Coccioni, 2013). The closure of Tethys marked the beginning of the compressional phase, which led to the formation of the Alps since the Cretaceous (e.g., Dewey et al., 1989; Schmid et al., 2004; Stampfli & Borel, 2002; Handy et al., 2015), the Dinarides-Albanides since the Palaeocene-Eocene (e.g., Ustaszewski et al., 2010; van Unen et al., 2019; Schmid et al., 2020; van Hinsbergen et al., 2020), and the Northern Apennines since the Oligocene (e.g., Molli, 2008; Molli and Malavieille, 2011; Barchi, 2010; Caricchi et al., 2014; Carboni et al., 2020 a, b). The migration of both the Dinarides and Apennines towards the central axis of the Adriatic Sea (Channell et al., 1979), led to the deposition of upper Eocene–Quaternary sequences on their common foreland basin.

The stratigraphic succession includes a Mesozoic–Paleogene, pre-orogenic, passive margin succession, deposited on the southern side of Western Tethys, and a Neogene–Quaternary, syn-orogenic succession, deposited on the flexured foreland of the Northern Apennine. A reference stratigraphic column is shown in Figure 2, illustrating the main units derived from Pesaro Mare 4 and W 1 boreholes drilled in the study area (Fig.1).

The uppermost unit includes up to ~ 3200 meters of Pliocene–Quaternary foreland turbiditic clastic sediments, ranging from Upper/Lower Neritic to Pelagic Platform environments, and includes the Argille del Santerno (AS) and Porto Garibaldi (PG) formations. These sediments transgressively overly a relatively thin Miocene Marly Group succession, deposited in the distal part of the foreland. This succession includes formations of the Messinian’s Gessoso Solifera (GS) (relatively thin), Schlier (SCH) and Bisciaro (BIS) formations. The pre-orogenic multilayer, spanning from the Late Triassic to the Early Miocene, lies beneath the overlying successions. This interval consists of Meso-Cenozoic carbonate deposits alternating between platform and slope facies, indicative of deposition in Lower to Middle Neritic and Pelagic Platform settings. Key formations include the Upper Jurassic to Oligocene Scaglia (SCA), Marne a Furoidi (FUC), Calcari di Cupello (CDC), and Calcari di Asprigni (CDU), as well as Lower Jurassic dolostones, such as the Calcare Massiccio (MAS) and Dolomie di Castelmanfrino (DCM). Compared to the Umbria-Marche Basin, this succession shows significant differences, notably the interlayering of platform facies with pelagic deposits in the Late Jurassic to Early Tertiary interval. The Triassic succession of the Anidriti di Burano Formation (BF) consists of alternating dolostones, anhydrites, halite, and gypsum, and act as regional décollement horizons (Casero and Bigi, 2013). Beneath this succession, the pre-Mesozoic crystalline basement of the Adriatic microplate forms the foundational framework (Vannoli et al., 2014). Due to the limited availability of deep wells, direct data on the thickness and depth of these deeper units remain sparse, necessitating reliance on seismic interpretation.

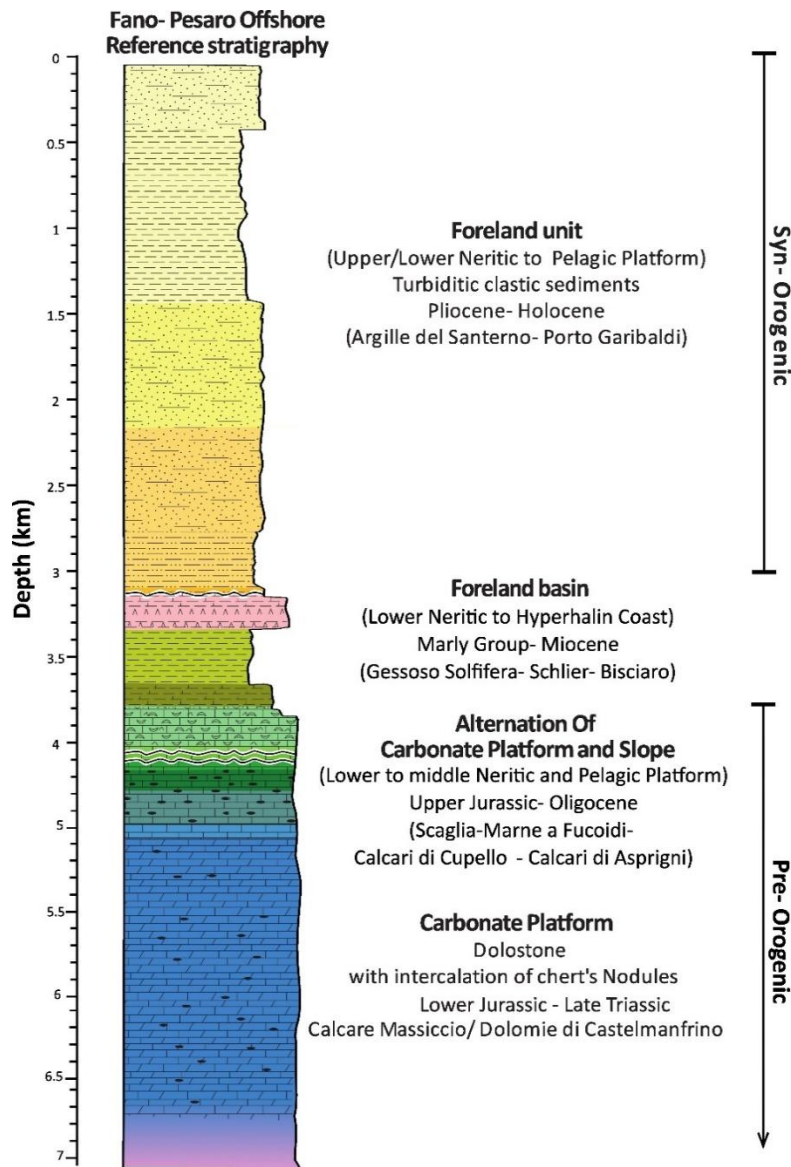


Fig. 2. Reference stratigraphic column for the Pesaro-Fano offshore area (from the Late Jurassic to Holocene sedimentary succession), derived from two representative boreholes (W1 and Pesaro Mare 04, location in Fig. 1).

The NA is characterized by high sedimentation rate, that in the Po Plain area reached more than 2.5 mm/year during the Calabrian, decreasing down to ~ 0.4 mm/year in the Upper Pleistocene (Maesano & D'Ambrogi, 2016). In the NA Sea, it is estimated in 1–2 mm/year in the Pliocene (Amadori et al., 2020; Ghielmi et al., 2013, Maesano et al., 2023). The high sedimentation rate, the absence of a clear seafloor deformation found on bathymetric and seismic reflection data (Di Bucci & Mazzoli, 2002), along with the generally low-to-moderate magnitude of instrumental seismicity ($M_w < 4.0$, before 2012),



have fueled the scientific debate on the recent activity of the external Northern Apennines. Contrary to slightly more internal sectors (e.g. Conero area, [Cuffaro et al., 2010](#)), most authors agree that the tectonic deformation in this external area might be hidden by such a fast sedimentation rate. In the NA Sea, the shortening rate is estimated in 1–2 mm/year until the Calabrian times, although some studies suggest spatial variations and a progressive temporal decrease ([Maesano et al., 2015](#); [Gunderson et al., 2018](#); [Amadori et al., 2020](#), [Panara et al., 2021](#)). Within the same area, some authors, using GNSS data from offshore hydrocarbon seabed-anchored platforms, recently calculated a present-day shortening rate, to be about 1.5 mm/year ([Palano et al., 2020](#), [Pezzo et al., 2020](#); [2023](#)). The offshore tectonic deformation characterizing the study area has been imaged by seismic reflection profiles, showing that the tectonic structures are organized in multiple blind thrusts with associated anticlines ([Argnani, 1998](#); [Bigi et al., 1992](#); [Fantoni & Franciosi, 2010](#); [Ghielmi et al., 2010](#); [Maesano et al., 2023](#)). Such reverse faults are buried below thick Plio-Pleistocene marine and continental deposits and likely rooted at depth along a common basal décollement ([Bally, 1986](#), [Panara, et al., 2021](#), [De Nardis et al., 2022](#)).

The debate about the recent activity of the external Northern Apennine associated to such blind thrusts has been revived during the last ~ 15 years, as a few important earthquake sequences have been recorded before the 2022 sequence ([Maesano et al., 2023](#); [Lavecchia et al., 2023](#)): one in the 2012 and a second in the 2013, onshore in the Pianura Padana (northern Italy) and offshore southern of Ancona in Marche region, respectively ([Mazzoli et al., 2015](#), [Maesano et al., 2013](#); [Burrato et al., 2012](#); [Scognamiglio et al., 2012](#); [Tertulliani et al., 2012](#); [Pezzo et al., 2013](#); [Tizzani et al., 2013](#); [Bonini et al., 2014](#); [Nespoli et al., 2018](#)). Additionally, a revision of the historical seismicity extracted from the available seismic catalogues, reports sequences encompassing mainshock events of $M_w > 5.5$, whose epicentres location is mapped either offshore or onshore the coastline (e.g., 30 October 1930 M_w 5.8 at Senigallia ([Vannoli et al., 2015](#)), Fig. 1). These earthquakes have been mainly caused by active thrust faults and produced several induced effects as well as victims and extensive damages within the Marche Region ([Guidoboni et al., 2019](#), [Rovida et al., 2022](#) and [Locati et al., 2022](#)). All these recent seismic events stimulated recent studies integrating different disciplines, providing new information, evidence and constraints to the active tectonic setting of the outer Northern Apennines

3. Fano-Pesaro earthquake: State of the Art

Most authors identify the Adriatic domain being mainly governed by compressive tectonics, with thrust-related deformation playing a dominant role (e.g., [Pauselli et al., 2006](#); [Maesano et al., 2013](#); [2023](#); [Sani et al., 2016](#); [Lavecchia et al., 2023](#)), although others suggest the region is primarily affected by active strike-slip tectonics, with minor thrusts occasionally reactivated (e.g., [Di Bucci and Mazzoli, 2002](#); [Mazzoli et al., 2015](#)).

Since the Fano-Pesaro 2022 earthquake sequence, new research has been conducted to map the existing structures and recognize the possible seismogenic faults through several hypotheses and scientific approaches as well as improving the accuracy of seismicity relocation ([Maesano et al., 2023](#); [Pezzo et al., 2023](#); [Lavecchia et al., 2023](#); [Pandolfi et al., 2024](#); [An et al., 2024](#)).



Maesano et al. (2023) performed a review and reinterpretation of public seismic reflection profiles (CROP and ViDEPI profiles), alongside comparisons with earthquake locations and aftershock distributions from INGV. These authors suggested that the Fano-Pesaro Offshore earthquake sequence took place on a relatively small section (25-40 km²) of the buried Cornelia Thrust System (CTS), situated at the edge of the Northern Apennines (Fig. S1). They also proposed a control by pre-existing normal faults and associated structural highs of the subducting Adria monocline (Amadori et al., 2019; Livani et al., 2018). Their work confirms the CTS being an active fault, It is roughly 300 km² in size, which could produce ruptures up to magnitude 6.5 and may trigger nearby faults.

Pezzo et al. (2023) characterized the seismic sequence in space and time, using data from the INGV monitoring system, GNSS-constrained coseismic slip, and public seismic reflection profiles (ViDEPI). They observed shallow buried anticlines in the upper 5-6 km of the crust with ramps dipping 20°–35° extending from a deeper, regional basal décollement with a westward dip of 1°–7°. Based on the distribution of relocated aftershock events, the authors interpreted a 15 km long striking seismogenic fault patch, dipping 24° SSW and seismically active at depths of 5– 10 km. Their mainshock relocation generated a 4.4 km shift to the south and a depth increase down to 8 km.

Lavecchia et al. (2023) examined the multi-scale geometries of slowly deforming continental regions (SDCR) in eastern Central Italy, focusing on lithospheric-scale deformation (De Nardis et al. 2022). They suggested the presence of a shallow megathrust (T1, ~ 20 km to few km deep) which represents the basal detachment of the external fold-and-thrust domain of the Adriatic Arc. These authors propose the T1 splay, named Bice thrust, extending ~ 30 km with a listric geometry (dip angle ~ 40°– 20°, seismogenic depths ~ 7– 11 km) and converging at depth with the Cornelia Thrust. Upon associating the first mainshock (Mw 5.5) with the central and southern part of the Bice thrust, they interpret the second event (Mw 5.2) due to the subordinate activation of the northern part of the Cornelia Thrust. Following this study, Pandolfi et al (2024) conducted a probabilistic seismic hazard analysis for the Adriatic Thrust Zone (ATZ).

An et al. (2024) proposed a new workflow to relocate the Fano-Pesaro seismicity clusters in a depth range of 2–12 km, with a best-fit dip of about 30° towards the south-southwest. In comparison to the results available in the INGV catalogue, they presented a sharper earthquakes cluster closer to the shoreline, mapping a geometry coherent with the available focal mechanisms as well as with the horizons interpreted in seismic reflection profiles.

While the approaches, results and interpretations on thrust geometries, dimensions, depths and structural relationships might differ, all the above-mentioned studies agree that 2022 earthquakes are related to an averagely ~ 30° dip, southwest-dipping thrust fault, located in the frontal part of the Northern Apennines. However, different opinions remain about which thrust could be the causative structure for the recently recorded seismicity.

4. Data and methods

The findings outlined in this paper are based on the interpretation of four deep wells (Table 1) and a set of seismic reflection profiles covering an area of approximately 1400 km², five of which are described and discussed in detail. No digital data (e.g. SEG-Y files) were available to be used for enhancing the quality of the dataset (e.g., Barchi et al., 2021, Ercoli et al.,



2023, Carboni et al., 2024), but all the seismic reflection profiles were provided as digital images, scanned from hard paper copy, in pdf format. Three of the selected seismic reflection profiles and a key-borehole, kindly provided by the Italian Energy company Eni S.p.A. under a confidential agreement, are unpublished. The other boreholes and seismic reflection profiles were retrieved from publicly available datasets from ViDEPI databases (<https://www.videpi.com>; <https://www.crop.cnr.it>) (Figs. 1 and 2, Table 1), along with industrial exploration reports and maps, which have been deeply reviewed.

A workflow, including different steps to gather and analyse all the data and ancillary information, has been set up:

1. *Data preparation*: data organization, quality control (QC), digitalization, georeferencing and importing into a geoscience multi-discipline integration software. 2D and 3D visualization of seismic reflection profiles, wells stratigraphy (formation tops), log images, and seismicity.
2. *Data integration*: stratigraphic correlation among the wells' tops and logs to identify a local seismic stratigraphy, well-to seismic tie analysis and seismo-stratigraphic interpretation.
3. *Velocity model building*: a key well sonic log (Table 1) was used to extract velocities for Pleistocene and Pliocene formations, whilst literature velocities were adopted for deeper layers (older than Late Miocene).
4. *Time to depth conversion*: horizons, faults and surfaces were converted to depth and the correlations were extended and verified across a broader area.
- 5.

Table. 1. List of datasets (Sp= Spontaneous Potential, Res= Resistivity, Sn = Sonic). The star* marks the unpublished data, obtained under a confidential agreement, the hashtag# reports the public data downloaded from the Italian database ViDEPI.

Seismic profiles				Wells		
Type	Name	Length (Km)	Notes	Name	Depth	Logs
Cross line (NE-SW)	S1*	18	Intersected by W1 well	W1*	4300 m Reached the Lower Cretaceous (Calcari Di Cupello (CDC) Fm).	Sp, Res
	S2*	11.5	Adjacent to main shock (134 m)			
	S3# (B-402)	30	/	Tamara 01#	3191 m Reached the Lower Miocene (SCH Fm)	Sn, Sp, Res
	S4# (SV-167-13)	21	Intersected by Cornelia well	Pesaro Mare 04#	4258 m Reached the Lower Jurassic Dolostone (MAS Fm).	Sp, Res
Tie line (NW-SE)	S5*	22	Adjacent to Pesaro mare 04 well	Cornelia 01#	3976 m Reached the Lower Jurassic Dolostone with Chert (Non defined ~ MAS Fm).	Sp, Res



5. Results

5.1. Wells' stratigraphy

The wells' stratigraphy was digitized, analysed to identify common geological characteristics (e.g., stratigraphy, lithology, discontinuities, petrophysical properties derived from the logs) and trends (formation thickness, spatial continuity) among the wells. After reviewing and correlating the lithological and structural information among all the data, a reinterpretation of the wells' stratigraphy has been accomplished and displayed in Figure 3. In the latter, the analysed wells are displayed sequentially, moving from the northwest to the southeast of the study area (Table 1, red arrow in Fig.3a). The data has been summarized, aiming to clearly show the tectono-stratigraphic correlation among the four wells, highlighting the spatial variation and gaps due to the presence of erosional and tectonic discontinuities (Fig.3b). Aiming to a deeper understanding of subsurface geology within the study area, such well information was spatially extrapolated along the available seismic reflection profiles, by correlating them with the interpreted TWT (Two-Way Travel Time) seismic horizons ("well- to-seismic tie", Bianco, 2014) and fault sets.

The W1 well intersects the easternmost segment of the seismic profile S1, containing 160 m of Lower Cretaceous carbonates. Within this well, three erosional boundaries are identified, corresponding to the Messinian, middle-lower Paleocene, and Lower Cretaceous tops (Fig.3).

The Tamara 01 well, located 600 m southeast of the seismic profile S2 and near the epicenter of the 5.5 Mw mainshock of the 9th November 2022, provides valuable sonic log data for deriving interval velocities and conducting well-to-seismic tie analysis. Projected orthogonal onto the eastern segment of the S1 and S2 seismic profiles, Tamara 01 well penetrates the upper Miocene SCH Formation for about 176 m. The well exhibits four erosional and two tectonic boundaries. The erosional boundaries are identified within the Lower Pleistocene at depth of 1217 m and at two levels marking the tops of the Upper Pliocene (1370 and 1912 m) and one level marking the top of the Upper Miocene, located at depths of 3015 m. The two tectonic boundaries are recognized from the repetition of the Miocene-Pliocene sequences at depths of 1743 and 2345 m, respectively (Fig.3).

The well Pesaro Mare 04, situated approximately 1 km southwest of the S3 profile, was projected orthogonal onto it. The well penetrates the sequence down to the Lower Jurassic, encompassing 1729 m of dolomitized MAS. Notably, an erosional boundary corresponding to the Miocene top is documented in the well stratigraphy at a depth of 372 m (Fig.3).

The Cornelia 01 well, located in the southeastern part of our study area, intersects the seismic profile S5. It penetrates Jurassic dolomitized carbonates, which are originally referred to an *undefined* formation based on the lithological variations and on the reported depositional environment; however, it is equivalent to the Dolomie di Castelmafrino (DCM) formation. This well exhibits five erosional boundaries corresponding to the tops of the Upper Pliocene (686 m), Lower Pliocene (738 m), Upper Miocene (790 m), Upper Cretaceous (1833 m), and Lower Cretaceous (2478 m). Additionally, a tectonic boundary is reported approximately 30 m from the bottom of the well. It is interpreted as a thrust splay, whose offset results in the repetition of the Early Cretaceous succession (Fig.3).

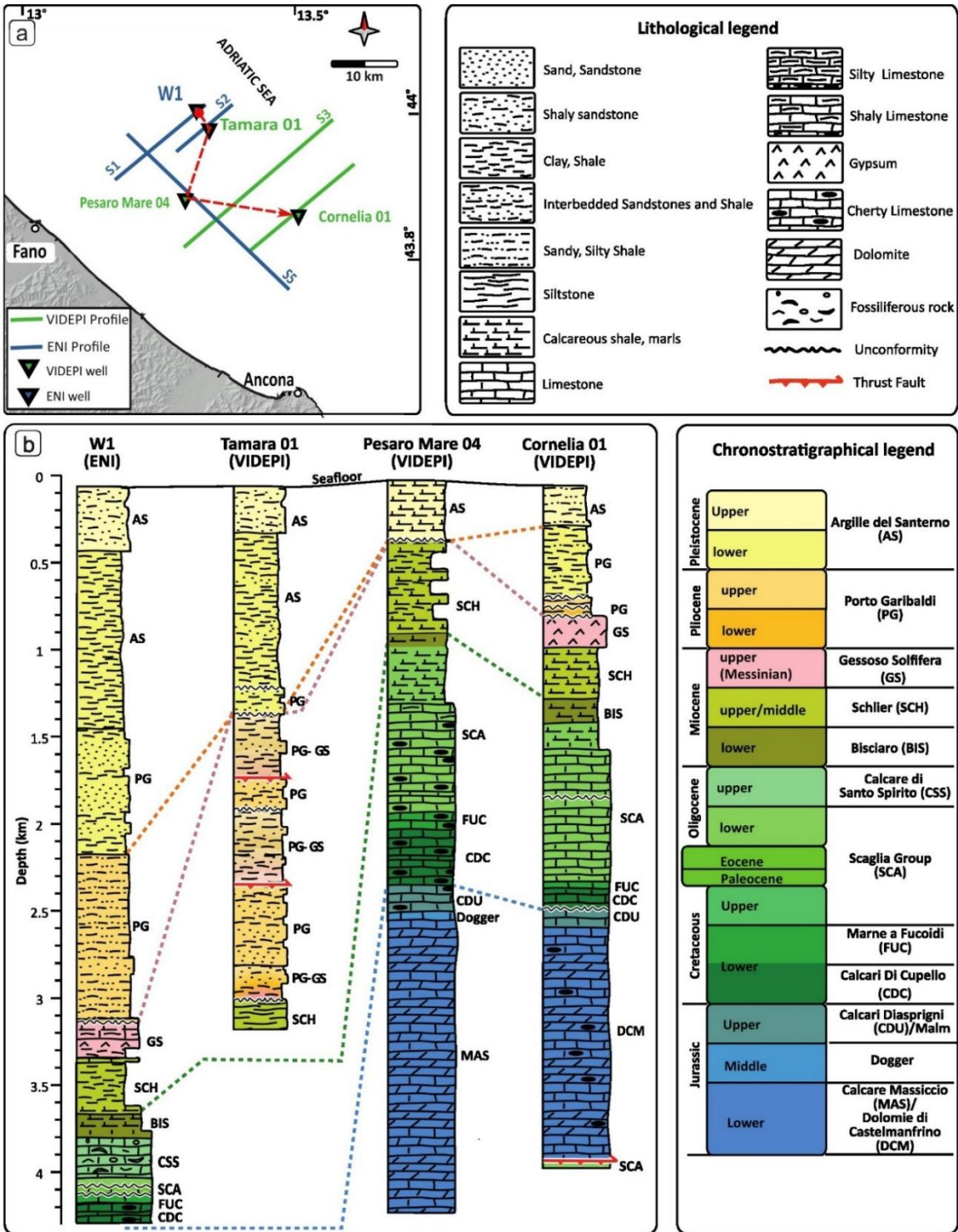


Fig. 3. a) Location map showing the position of the analysed wells. b) Schematic stratigraphic columns of the wells, reinterpreted from the original data in the ViDEPI database and arranged spatially from northwest to southeast (red arrow in Fig. a).



275 From the global analysis of the four wells' data across the study area (Fig.3), the Pliocene-Quaternary successions show a significant thinning from ~ 3100 m thickness in the northwest to 400– 700 m in the southeast, as recorded in Pesaro Mare 04 and Cornelia wells, respectively. Within this succession, the Pliocene-Pleistocene sedimentary sequence is frequently incomplete. Notably, in the Pesaro Mare 04 well, situated on a structural high, the Pliocene succession is entirely absent, with a direct transition from Miocene deposits to Quaternary sediments. Conversely, in the basin areas, such as the W1 well, 280 a more complete sequence spanning the lower to upper Pliocene is preserved. This sequence is characterized by alternating sandy and clayey layers, often interbedded with marly components. This sequence unconformably overlies the Messinian (GS) evaporites, which are identified exclusively in the northwestern and southeastern wells of the study area. These evaporites are associated with a Messinian paleo-high that persisted as a subaerially exposed feature for the majority of the Pliocene (Report 1508, ViDEPI).

285 The lithological analysis of the Meso-Cenozoic carbonate successions within the studied wells reveals a carbonate platform that underwent progressive deepening, testified by the combination of detrital and dolomitic limestones, interspersed with frequent cherty nodules and marly intercalations, particularly in the lower sections. The Triassic succession (BF), which typically consists of evaporites and dolostones in the central Apennines (e.g., Umbria-Marche and Sabina Pelagic Basins), in this study area is almost entirely composed of dolostone facies, as reported by the analysed wells. This is also shown by the 290 Alessandra 1 well, located slightly to the east, which represents the deepest borehole drilled in this region (Bally, 1986; Carminati et al., 2013). As the succession transitions into the Middle Jurassic and extends to the Paleogene, the limestones gradually give way to marly layers, again characterized by typical nodular structures. Additionally, clastic intercalations are observed, suggesting sedimentary inputs from the erosion of adjacent structural highs. Notably, the thickness of the SCA Group increases significantly from the northwestern to the southeastern studied wells

295 5.2. Seismic stratigraphy and time-to depth conversion.

By correlating and calibrating the stratigraphy of Tamara 01 and W1 wells with all the available seismic profiles, we have identified five primary seismic units (SUs), bounded by four prominent, easily traceable key-reflections. These units exhibit distinct geophysical signatures, such as variation in the reflection amplitude, period and geometry. The analyzed seismic profiles follow SEG normal polarity, meaning that an increase in acoustic impedance is represented by a peak, while a 300 decrease corresponds to a trough. The SUs are discussed in the following from top to bottom (Fig.4 and details within the Supplementary Table S1).

The Holocene-Pleistocene turbidites (SU1) comprise fine sandstones, shaly sandstones, and interbedding of shale and silty shale pertaining to AS. SU1 consists of four distinct seismic sub-units (SU1 a, b, c, d), each one characterized by a different seismic signature (see supplementary Table S1). SU1 a, b are characterised by seismic facies from continuous to semi 305 discontinuous horizontal and parallel reflections, with low to high amplitudes; the bottom SU1 c, d display continuous to



semi-continuous E-dipping reflections, with medium to high amplitudes. The total thickness of this unit gradually increases north-eastwards from 0.2 s to 0.3 s (Fig. 4 and Supplementary Table S1).

SU2 is separated from SU1 by a top-lap unconformity, dated Top Gelasian (Fig. 4) referring to early Pleistocene older than 1.8 Ma. The Gelasian turbidites within the upper part of PG consist of silty shales with interbedded shales at the top, transitioning to fine sandstones and shaly sandstones in the lower part. The thickness of this unit gradually increases from 0.2 s in the SW to 0.6 s in the NE. Within SU2, we identified two sub-units (SU2 a, b), each one characterized by distinct seismic signature. The uppermost sub-unit (SU2 a) shows continuous E-dipping parallel reflections, with medium to high amplitudes. In contrast, the lower sub-unit SU2 b features semi-continuous, parallel, and sub-horizontal reflections (Supplementary Table S1).

The Pliocene turbidites (unit SU3) within the lower part of PG are composed of silty marls intercalated with medium to very fine-grained sandstones. The subunits (unit SU3 a, b, c) display distinct reflection patterns. The uppermost subunit (SU3 a) exhibits continuous, horizontal, parallel reflections with high amplitude, while the other subunits (SU3 b and SU3 c) show discontinuous to semi-continuous, sub-parallel reflections with low to medium amplitudes. Their thickness variation across different sections is ranging from a few ms to 0.4 s (Fig. 4).

The complex Miocene succession (SU4) found within the SCH, and BIS, are composed of shales and marls interbedded with siltstones, carbonates, and minor gypsum deposits. This marly group displays continuous, parallel reflections with high amplitude and dominant frequency in the narrow uppermost part; the rest of the unit presents continuous to discontinuous, sub-parallel reflections with medium to high amplitude. This seismic unit progressively deepens from southwest to northeast. The high amplitude and dominant frequency within this unit create distinct and sharp reflections in the seismic sections.

The Mesozoic-Paleogene carbonate multilayer (SU5) unit corresponds to the SCA, MAS and DCM, and represent the deepest recognized units. The unit consists of limestone and dolomitized limestone, with intercalations of marls and chert nodules. Notably, it exhibits a substantial thickness of over 1 s. The reflections within this unit display a discontinuous, sub-parallel pattern with low to medium amplitude and are marked by some continuous, high amplitude and well-recognizable reflections which are related to the top of the SCA and FUC fms. (Mirabella et al., 2008; Porreca et al., 2018; Barchi et al., 2021).

For the depth conversion, a velocity model has been built, by integrating new interval velocity values derived from the sonic log of the Tamara 01 well (down to the Late Miocene turbidites) with literature velocity data (e.g., Bally et al., 1986; Maesano et al., 2013, 2023; Montone and Mariucci, 2023). Bi-dimensional velocity models were initially built up along each single profile, with a focus on the shallower area (down to the Top Scaglia). This workflow was then extended across a tri-dimensional workspace, encompassing later variations driven by all the picked horizons and faults surfaces, and considering some control points corresponding to wells located a broader area. Such a velocity model was later refined in its deeper portion (down to the Jurassic carbonate units) and used to carry out the final conversion from the time to the depth for all the selected seismic profiles. Further details on the velocity models are provided in the Supplementary Table S2.

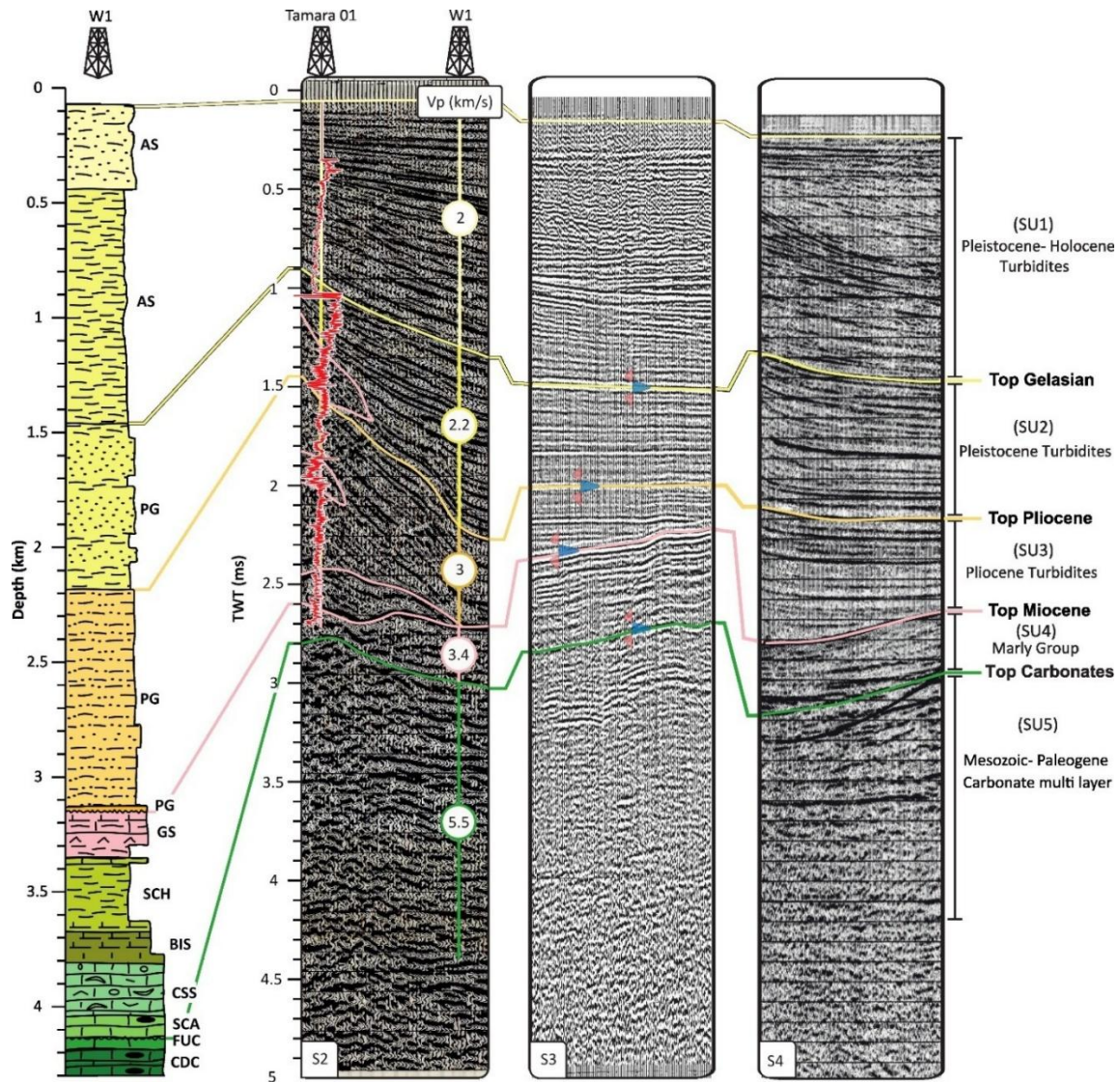


Fig. 4. Seismic stratigraphy of the study area (colored lines) calibrated using the Tamara 01 and W1 wells, (see Fig. 1 for well locations and Fig. 3 for stratigraphy column abbreviations). Vp indicates the P wave seismic velocity. Additional details are provided in the text and supplementary Table 2.

5.3. Seismic interpretation

To provide an accurate representation of the subsurface geological and structural features within the research region, five seismic profiles have been selected to carry out the seismic interpretation. Their location and details are reported in Figures 5, 6 and Table 1, while the uninterpreted versions can be found in the supplementary material (Figs. S1 and S2). The dataset includes four SW-NE-oriented “cross-lines” (S1, S2, S3, and S4) and one NW-SE oriented “tie-line” (S5). The SW-NE profiles cross the two major anticlines present in the area, namely the northern Pesaro Anticline (PA) and the southern



350 Cornelia Anticline (CA), developed at the hanging walls of SW-dipping thrusts, named Pesaro thrust (PT) and Cornelia thrust (CT).

The whole interpretation of seismic profiles has been realized by using a tri-dimensional correlation of key reflections picked along the single seismic profiles, with respect to seismic-stratigraphic units obtained from the well-tie analysis. In this section, the description of the seismic profiles is done from northwest to southeast. The profiles are described considering the increasing TWT (s) and their along line distance (km).

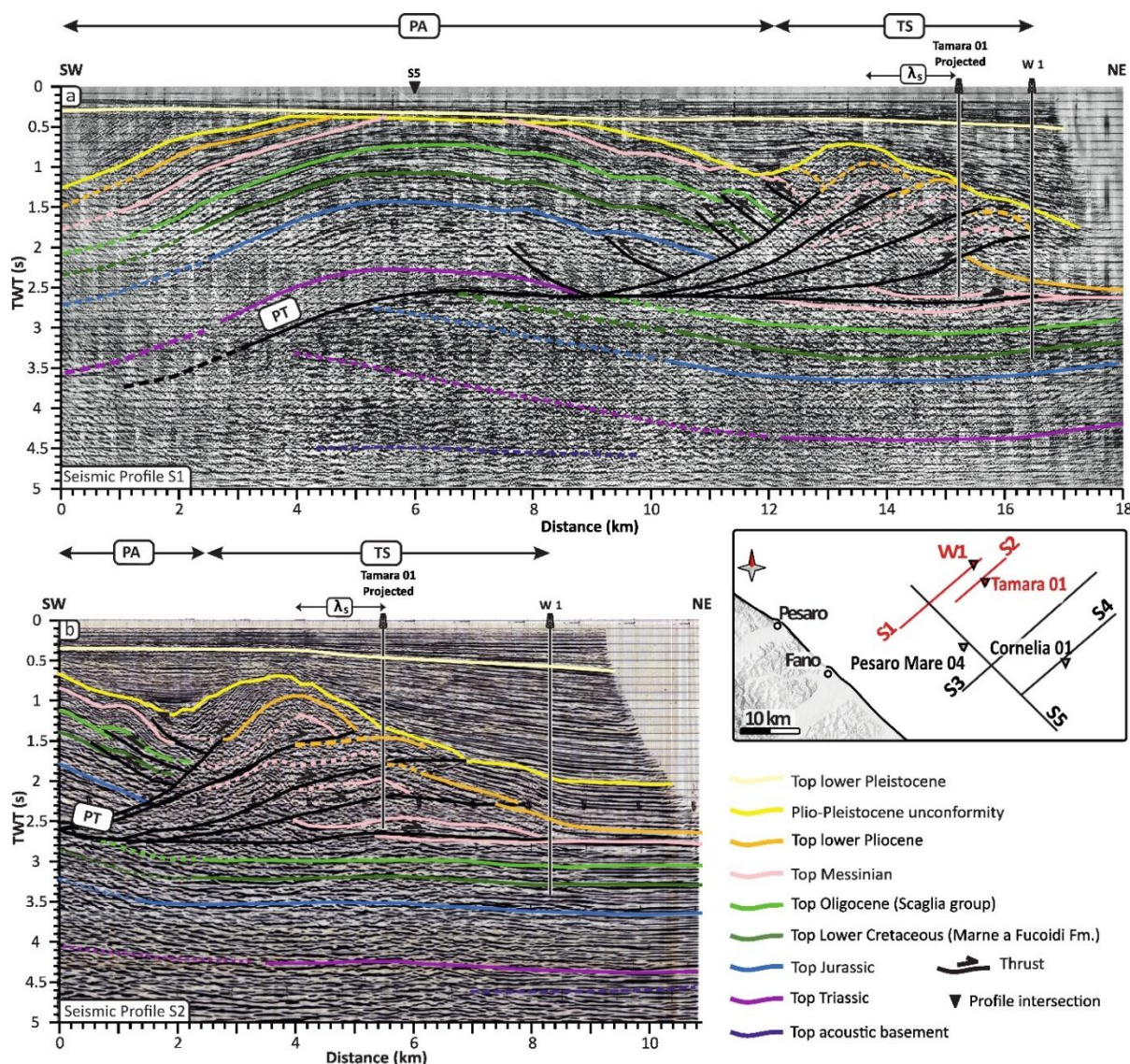
The seismic profile S1 in Figure 5a is dominated by the east-verging PA, characterized by a long wavelength of ~ 13 km (0–12 km distance, Fig. 5a). The PA geometry is traceable from ~ 0.2 s down to ~ 2.5 s, and it is particularly evident following the interpreted Top Jurassic to Top Messinian reflections (blue and pink colours, respectively). To notice that the Top Messinian reflection is not traceable in the culmination of the PA anticline, due to erosion; in addition, a set of minor folds characterize the PA forelimb (9–12 km distance range). Further to the northeast, between 12 and 17 km distance, a complex antiformal structure (wavelength ~ 5 km) folds the Plio-Pleistocene unconformity reflection (dark yellow colour).

This antiformal stack involves a set of minor imbricates, with wavelength < 1 km, detached above the Top Carbonates (Oligocene) reflection (light green colour). The antiformal stack is here referred to as the Tamara structure (TS), drilled by the Tamara 01 well. The PA and TS are separated by a short wavelength (~ 4 km) syncline (~ 9–13 km distance), which is infilled by sub-horizontal reflections interpreted as lower Pliocene sediments, onlapping onto the Plio-Pleistocene unconformity (Fig. 5a). In the northeastern part of the profile (~13–17 km), a clear increase in the apparent dip angle and thickness of the Pliocene succession reflections is visible. Both the PA and the TS are interpreted to be situated in the hanging wall of the SW-dipping main PT thrust. The hinge zone of PA is located on top of the main PT ramp, located within the Mesozoic succession; this ramp links its deepest part with the shallowest, flat portion at ~2.5 s (Fig. 5a). However, in this forelimb sector, a set of imbricate forethrusts and backthrusts have been interpreted departing from PT. These backthrusts have been associated with the minor folds described above on the PA forelimb (~9–13 km distance range). Such backthrusts are detached along the shallower, most internal PT ramp. On the other hand, the set of imbricate forethrusts, build up the shorter wavelength TS and they are all detached along the PT shallower flat. The three imbricates displace up to the Top Messinian and the Top lower Pliocene reflections of at least ~0.1 s TWT, but not the Plio-Pleistocene unconformity, which is only folded. The presence of such imbricates is also interpreted and constrained by the Tamara 01 well stratigraphy, clearly showing two repetitions of the Top Messinian. Further constraints on the PT geometry derive from a set of parallel sub-horizontal reflections observed between 2.5 s and 3.5 s (5–18 km range); they are discordant with the shallower reflections, especially in correspondence with the main ramp, between 3 and 8 km distance, where they look slightly E dipping. These reflections would represent the PT footwall succession, up to the Top Messinian (Fig. 5a).

380 The seismic profile S2 (Fig. 5b) gives a clearer picture of the TS imbricates. Projecting the Tamara 01 well and picking the Top Messinian reflections, the presence of three imbricates within the TS, which produce three repetitions of the Messinian and Pliocene successions, have been interpreted. The imbricates are detached on the shallow PT flat (~ 2.5 s TWT), which produces a further repetition of the Top Messinian reflection (pink colour). In the south-western part of S2, again the minor



385 folds driven by the backthrusts mapped in S1 are observable in the north-easternmost part of the PA forelimb. Within S2, like in S1, the growth deposition of the Pliocene succession is also observed in the northeastern part (apparent E-dip), and the syncline separating the PA and the TS, again characterized by parallel sub-horizontal reflections associated with the Pleistocene unit (Fig. 5b).



390 **Fig. 5.** Interpretation of S1 and S2 seismic profiles. a) S1, the northernmost section in the study area, crosses the left hinge zone of
 the PA and reveals variations in its structural style. The geometry of the PA is evident by using the Top Messinian, Top Oligocene
 and Top Lower Cretaceous reflections. The section also shows TS shallow seated structure developed laterally to the South-
 Eastern termination of the PA. b) S2 shows the enhanced comprehension of the TS's underlying structure. Four imbricated
 395 thrust zones of the PA forelimb and the repetition of Messinian- middle- lower Pliocene successions are observable
 (uninterpreted images provided in supplementary materials, Fig.S1).



The seismic profile S3 (Fig. 6a) provides an excellent view of the structural relationships between the two main structures of the area: the main thrusts PT and CT with their related anticlines PA and CA. The PA is displayed in the southwestern part of the profile (0–10 km distance range). Its geometry can be easily appreciated by following the Top Jurassic to the Top Messinian reflections (blue and pink colours, respectively); the latter is again partially eroded in the axial zone. A few smaller antiformal structures located at the PA forelimb, as already observed in S1 and S2, are again interpreted as being driven by small backthrusts. This profile also shows a strongly reduced size of TS and a steepening of the PT here partially overlies the western flank of another anticline, identified as CA. More north eastwards, the latter appears as an asymmetric NE-verging anticline, traceable from ~ 0.8 s down to ~ 3 s. This anticline is interpreted being related to the underlying CT, whose location is constrained by the Cornelia 01 well. The CT displaces the Meso-Cenozoic succession up to the Top lower Pliocene reflection (orange colour), while the Plio-Pleistocene unconformity (yellow colour) appears only folded. The CT footwall is recognized following the Top Jurassic to the Top Messinian reflections, which are interpreted slightly parallel and W-dipping until around 18 km distance at ca. 3 s. The CT is interpreted to comprise also a small synthetic thrust, developed at its footwall, which produce a further repetition of the Top Scaglia Group and Top Messinian reflections. More to the northeast, we observe a shallower and thick package of growth strata, interpreted to comprise Pliocene to Quaternary deposits.

The seismic profile S4 (Fig. 6b), located at the southernmost extent of the study area, offers valuable insights into the internal structure of the CA and intersects the Cornelia 01 well, providing key stratigraphic correlations. In contrast to S3, the PA is not present in this seismic section. The CA is represented by an asymmetric NE-verging anticline (as already observed in S3), extending from ~0.5 s to ~3.5 s, and prominently displayed between 3 km and 14 km distance. This anticline is defined by the Top Jurassic up to the Pliocene-Pleistocene unconformity reflections (blue and yellow colours), situated within the hanging wall of the underlying CT. The latter, like in S3, offsets the Meso-Cenozoic succession up to the Top lower Pliocene reflection (orange colour). A small synthetic thrust is again observed in the footwall of the CT, which results in the repetition of the Top Scaglia Group and Top Messinian reflections over 9 to 14 km, extending to ~2.7 s. In the northeastern part of this section, the interpreted Pliocene to Quaternary deposits are thicker than in S3, with the top of the Pliocene reflection located at ~2.5 s. Additionally, S4 reveals minor fore-verging thrusts in both the southwestern and northeastern sectors of the section (Fig. 6b, at distance ranges 0–3 km and 15–20 km, respectively). While the two west-dipping convergent thrusts observable to the south-west of CA intersect and slightly displace the Messinian until the Plio-Pleistocene unconformity, the minor thrust to the northeast of CA is detached at the top of the Lower Cretaceous (~ 3.5 s to 2.2 s), displacing the overlying sedimentary successions including the Messinian and Lower Pliocene deposits (orange colour, Fig. 6b).

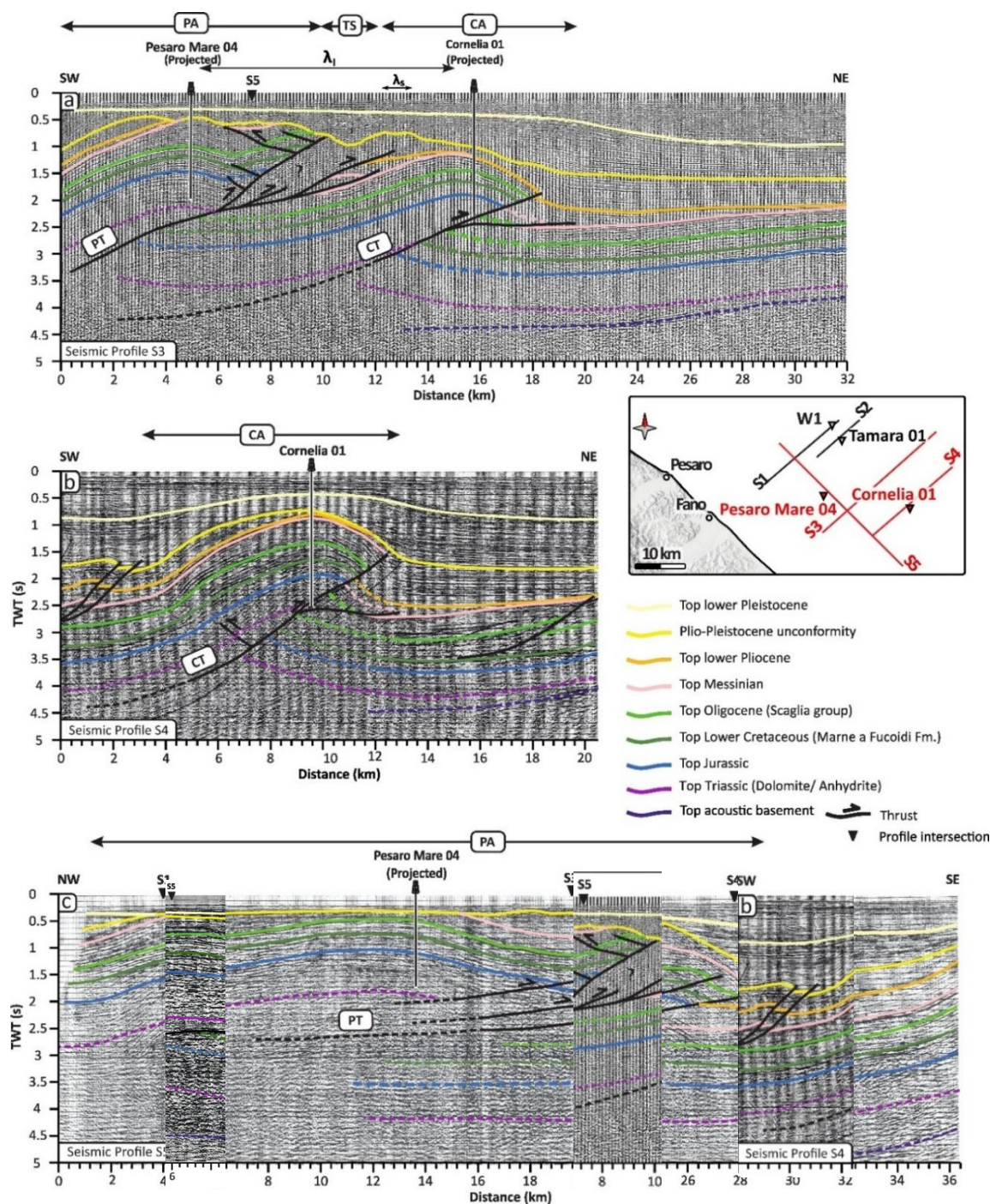


Fig. 6. Interpretation of seismic profiles S3, S4 and S5. a) Section S3 crosses the transition zone of PA and CA structures. The geometries of the anticlines are identified by using the key reflections (See the legend). However, in this section, the main reflections in the TS are not clearly traceable (the area marked with a question mark). b) Section S4 is the southernmost section that shows the CA. The doubling of the Mesozoic-Paleogene carbonate multilayer is observable in the frontal part of the CA. c) Section S5 is a tie line, crossing the crest zone of the PA (Uninterpreted images provided in supplementary materials, Fig.S2).



The seismic profile S5 (Fig. 6c) serves as a tie line, crossing the crest zone of the PA and situated approximately 500 m from the Pesaro Mare 04 well. This profile provides extensive areal coverage (~36 km), intersects the S1, S3, and S4 seismic profiles. It is essential for understanding the structure of the PA and **for conducting a 3D correlation of interpreted horizons among the aforementioned cross-lines**. The geometry of the PA is identifiable from ~0.5 seconds to ~2 seconds, being particularly prominent following the reflections Top Jurassic (blue) and the Top Messinian (pink). The Top Messinian reflection is visible in the northwestern and southeastern hinge zones of the PA, but is clearly absent in the axial zone (~ 4–15 km distance) due to erosion. The central portion of the PA (~12–29 km distance range) exhibits a stack of imbricate thrusts slices between ~1.5 s and ~2.5 s. These slices are characterized by semi parallel, closely spaced reflectors (Fig. 6c). The PA lies in the hanging wall of the PT, and it is significantly uplifted, forming a semi-symmetrical structure. In contrast, the footwall remains relatively undeformed. These three interpreted thrust faults cut across both the Mesozoic and Cenozoic successions. In the northwestern hinge zone of the PA, no clear displacement has been observed and interpreted within the primary reflections. Moving to the southeast, starting from ~ 16 km along the profile, growth deposition of the Pliocene-Pleistocene succession becomes increasingly evident. The profile highlights the superimposition of the Meso-Cenozoic sedimentary sequence over the Messinian reflection picked on top of the footwall, with clear evidence of duplication. The described interpretations carried out on the seismic profiles in TWT, have been then converted to depth, by using the integrated velocity model illustrated in figure 4.

6. Discussion

The integration of a new set of unpublished and publicly available seismic profiles with borehole data allowed to highlight the presence of deep-seated and shallow-seated tectonic structures, involving different lithologies and detached in correspondence of different décollements. This structural setting defines the geometry, dimension and segmentation of the main compressional structures, and ultimately their seismotectonic significance. Depth-converted profiles are used to discuss the possible link between the deep-seated tectonic structures and the seismicity of the area, with a focus on the 2022 seismic sequence (Fig.7). Three depth-converted seismic profiles, S1, S3 and S4 have been selected, being the most representative on the base of the achieved geological interpretation and aiming to build up a new geological model of the area (Fig. 7). These profiles cross perpendicularly the main structures and extend along the study area from the northwest toward the southeast. This orientation allows to observe the structural relationships between Pesaro Anticline (PA) and Cornelia Anticline (CA) and their thrust faults, Pesaro Thrust (PT) and the Cornelia Thrust (CT), providing a clearer view of the vertical and lateral distribution of the involved key stratigraphic units and of the tectonic features within the subsurface of the study area.



6.1. Multiple décollements and En echelon folds

465 In the area covered by this research, variations of mechanical anisotropy strongly influenced the structural setting, forming patterns of interconnected structures, detached along multiple décollements at different depth, corresponding to weak stratigraphic layers. Thus, the recognised tectonic structures have been grouped into two main categories: (i) deep-seated thrusts, represented by the innermost PT and the outermost CT (responsible for the formation of the large-wavelength structures PA and CA), which predominantly affect Mesozoic to Paleogene carbonate sequence; and (ii) shallow-seated thrusts, which are represented by closely spaced, short-wavelength structures of Tamara structure (TS), affecting only the Miocene sequence and its overlying turbidite deposits. The depth converted profile S1 provides a clear view of the spatial relationship among the aforementioned structures (Fig. 7a). PA is characterized by a NW-SE (along-strike) ~ 30 km long and is ~ 12 km wide (along-dip, SW-NE direction, see profile S1 in Figs. 5a, 7a, 7d). Its wavelength (λ) as defined by Massoli et al. (2006), thus measured between the PA and CA crests, is ~11 km (Figs. 6a, 7b). S1 shows PT being relatively flat in the shallow portion (~4 km), whilst westward of its steeper ramp; it is reasonable to image the PT lower décollement lying at around 9 km depth, possibly on top of the acoustic basement. However, as profile S1 doesn't extend more to the south-western sector, the interpretation of the deepest structures is poorly constrained, as based on its interpreted trajectory. S1 also shows a series of shallow imbricated, fore-verging and back-verging thrusts in the forelimb of the PA, forming TS, characterized by a length of ~10 km, a width of 7 km and a wavelength λ_s of ~1.1 km (Figs. 5a, 5b, 7a, 7d). All these structures are associated to the upper décollement extending nearly parallel within the Messinian marly group, at roughly 3.5 km depth. The fore-verging imbricated thrusts originated from the upper décollement of the PT within weak, marly rocks (ranging from the upper Miocene to Pleistocene), propagates both eastwards and upwards. This process resulted in multiple repetitions and duplications of the Miocene-Pliocene marly sequences. The nearby Tamara borehole further constraints our interpretation by drilling this shallower décollement close to the base of the Miocene "Marly Group" (Fig. 7a) and confirms the depth and the repetition of these sequences across at least three slices. Since the Tamara well was drilled on the outermost part of the Tamara antiformal structure, it does not drill the complete series of imbricated thrusts and duplicated sedimentary sequences mapped in S1 (Figs. 5a, 5b and 7a).

The overall analysis and observations of the seismic reflection profiles available on the southeasternmost extent of the study area, also allowed to describe the geometrical characteristics of CA, which are analogous to PA. It results in a NW-SE striking ~ 20 km long and ~ 12 km wide anticline (profile S4 in Figs. 6b, 7b, 7c) with a wavelength λ_l of ~ 11 km (Figs. 6a, 7b). These structural wavelength values, λ_l and λ_s , are larger than those obtained for corresponding structures in the Umbria-Marche area, where corresponding structures have wavelengths of 3.2 to 7.2 km for λ_l and 0.4 to 2.3 km for λ_s (Massoli et al., 2006), characterized by lower syn-tectonic sedimentation. Conversely, and they are smaller than those observed in the Po Plain, where higher syn-tectonic sedimentation contributes to even larger structural wavelengths, with λ_l ranging from 15.8 to 33 km and λ_s from 4.5 to 8.2 km (Massoli et al., 2006).

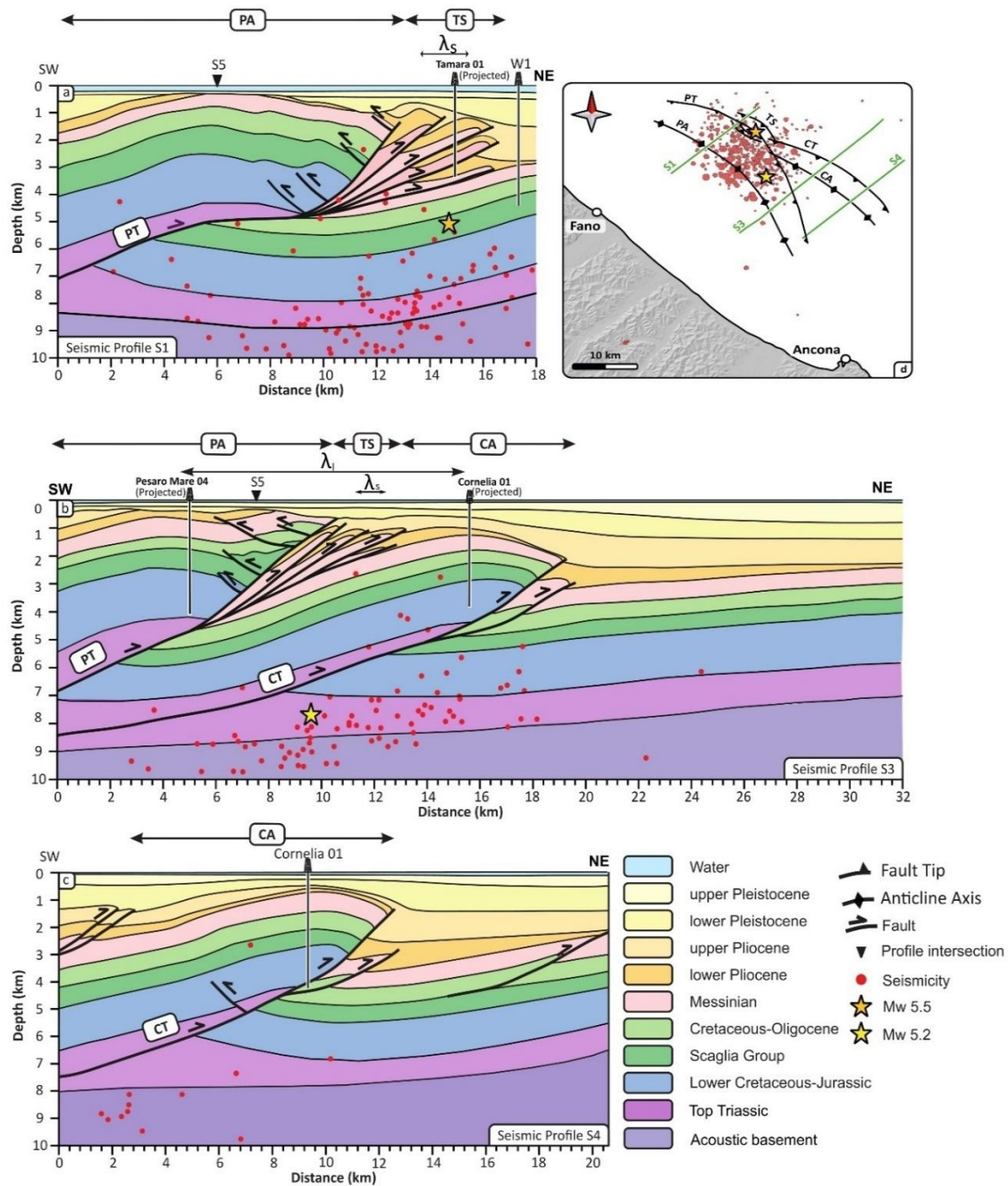


Fig. 7. Geological sections derived from: a) seismic profile S1, b) seismic profile S3, and c) seismic profile S4. The main shock of 5.5 ML and aftershocks are projected normal to the section within buffers of 5, 7, and 10 km, respectively. d) Location map of the interpreted anticlines and thrust faults (this work); the seismicity distribution is sourced from terremoti.ingv.it. λ_L : Wavelength of the large structures; λ_s : Wavelength of the small structures.

500



Our comparative analysis of the PA and CA anticlines, and their related deep-seated thrust systems PT and CT points out some structural similarities and **distinction**. From the analysis of the profiles S3 and S4 (Fig. 7b, 7c), looking at both anticlines geometry and the thrusts trajectories, **it is clear how the thrusts share a common deep décollement level**, at approximately 8–9 km depth (comparable to results in nearby areas provided by e.g., Pauselli et al, 2006, or Lavecchia et al., 2004). Furthermore, evidence indicates that the thrusting style in this area is a thin-skinned type of deformation, aligning with the observed décollement depth and suggesting tectonic processes that control syn-tectonic sedimentation and accommodate deformation within the overlying sedimentary cover, without involving the basement (Fig. 7). Our interpretation demonstrates that, unlike the PT, the CT lacks an upper shallower décollement. Instead, the ramp of the CT terminates blindly at a depth of 2 km within the base of the upper Pliocene turbiditic successions (Figs. 7b, 7c), and only one imbricated fore-verging thrust has been identified in S4. The latter is also constrained by the Cornelia borehole stratigraphy, evidencing a doubling of the early Cretaceous carbonate succession (Scaglia group) **over approximately 4 km**.

Considering the deeper structures involving the carbonates, this study documents the structural transition between two main compressional structures: the PA (internal) and the CA (external) anticlines. In map view (Fig. 7d), these structures are linked to a pair of en-echelon, vicariant, coalescent thrusts, the northernmost PT and the southernmost CT. The interpretation of the seismic lines clearly highlighted that the transition from PT and CT occurs through an intermediate region, where both structures are present (Fig. 7d) and can be viewed as adjacent segments of the outermost thrust of the Northern Apennines. Representative examples of coalescent anticlines extensively crop out also in the Umbria-Marche Apennines (Barchi et al., 1998; Scarsella 1941; Lavecchia, 1981; Lavecchia et al., 1988; Lavecchia et al., 2023), and such examples have been described worldwide since Dahlstrom (1970).

Our investigation shows that the shallow-seated TS structure **can be traced only in the southeastern termination of the deep-seated PA up to seismic Profile S3**, where both PA and TS overlap on the back limb of the CA (Fig. 7b). **However, in the southeastern part of our study area, as seen in seismic profile S4, the shallow-seated imbricated fore-verging thrusts and their related antiformal stacks (TS) are not observable (Fig. 7c)**. Our investigations indicate that the TS represents the deformed wedge of the frontal part of the PA structure, thus it cannot be considered originated by a single deep-seated structure such as PT or CT and neither a northwest-eastward continuation of the Cornelia thrust.

In slightly external sectors evidence of deep thrusts has been reported from the analysis of low-quality public profiles (Adriatic Arc Front, e.g., Bice thrust, Lavecchia et al., 2023). However, the present study suggests that the PT and associated imbricates did not extend more to the North-East. This consideration is also testified by the presence of a complete sedimentary succession (from Cretaceous carbonates to thick Quaternary sequences). Additionally, in the borehole W1 (drilled in the foreland of the PA), no thrust faults are reported and the Top Messinian reflection correlates well with the corresponding identified erosional boundary. Evidence of deeper, external fronts were not found in the reviewed commercial seismic reflection profiles available across this study area, possibly falling besides the data quality at depth or outside the data coverage.



535 **6.2. Seismotectonic implications**

The mechanical stratigraphy reveals that both the deep-seated PT and CT ramps cut through the brittle carbonate multilayer, from 3 down to 9 km depth. This range coincides with the depths of most of the seismicity recorded during Fano-Pesaro 2022 sequence (terremoti.ingv.it, Rovida et al., 2022), suggesting that these thrusts may potentially serve as seismogenic structures. Both PT and CT are southwest-dipping thrusts, with an interpreted dip angle of 30°–35°, compatible with the mainshocks focal mechanism (with strike 128°, dip 34° and rake 84°, terremoti.ingv.it).

Given their potential seismogenic role, the relationship between earthquake magnitude and subsurface rupture length for both the PT and CT was analysed using the regression diagrams (e.g. Wells and Coppersmith, 1994 and Leonard, 2014). Fault length directly influences the maximum possible displacement, and consequently, the potential maximum magnitude (Scholz, 2019). According to the findings of this analysis, the observed fault lengths are substantial enough to account for both recent and historical seismic activity in the region.

However, determining the exact causative faults for the 2022 November 9th earthquakes remains challenging. It is important to highlight the spatial mismatch (Fig. 1), in terms of both location and depth distribution, among the literature interpreted faults and the hypocentral records (terremoti.ingv.it). Comparing the published earthquake locations and relatively shallow depths (~ 5 km) with our new interpretation, seismicity is scarcely distributed across the Cornelia region (Fig. 7d). The first November 9th 5.5 Mw main shock appears more closely associated to the PT (extending more to the North-East), other than to the CT, the latter being less extended to the North-West (Fig. 7d). The second November 9th mainshock and the aftershocks fall in between the area covered by the seismic profiles S1 and S3, in the interpreted transfer area between PT and CT. This event is close to the PT zone and somewhat far from the CT's main area but occurring at greater depth (~ 8 km) in the footwall of the PT (Fig. 1, Fig. 7d). However, it is known that both earthquake hypocentres location and the depth of the “not-relocated” seismicity lack in accuracy, particularly in the offshore, due to the limited coverage of seismic stations. Recently, several authors has re-located the seismicity recorded during this 2022 sequence. Pezzo et al. (2023), An et al. (2024) and Costanzo (2024) used different relocation methods and methodological approaches and a significant uncertainty in defining seismic event depth compared to the location is noticeable.

560 **Table 2. Location and depth parameters of the mainshocks for the 9th November 2022 Fano-Pesaro earthquake, as determined by different sources.**

Event	Source	Depth (km)	Latitude	Longitude
Main Shock (Mw5.5)	INGV	5.0	43°58'59"N	13°19'26"E
	An et al., 2024	4.40	43°56'11"N	13°20'20"E
	Pezzo et al., 2023	7.94	43°59'41"N	13°18'58"E
Second Shock (Mw 5.2)	INGV	7.7	43°54'47.88"N	13°20'40.92"E
	An et al., 2024	8.4	43°51'36.36"N	13°20'16.44"E



The first relocation by Pezzo et al. (2023) shifted the main shock 1.5 km N-NW, increasing its depth to ~8 km, while aftershocks moved slightly NE and farther offshore. The second relocation by An et al. (2024) shifted the main shock 5 km southward, thus closer to the shoreline, with a shallower depth, and relocated the aftershock cluster 6 km S-SE. The spatial distribution of the relocated aftershock events, as well as the historical seismicity in this area, is farther from the CT and more concentrated around the PT and the transfer zone between the PT and CT (Figs. 1 and 7d).

This analysis underscores the complexity of determining whether the PT or CT served as a primary source of the 2022 seismic activity or if the latter might be associated to a possible deeper thrust (e.g., T1 as supposed by Lavecchia et al., 2023). However, such a possible causative fault is not imaged at depth within our available seismic reflection data, possibly due to the high level of random noise characterizing the legacy profiles (Ercoli et al., 2023) or due to the lack of reflected signals from deeper structures.

7. Conclusions

This paper presents a new geological model of the tectonic structures of the Fano-Pesaro offshore area within the frontal part of the Northern Apennines. Multiple décollements located at different depth have been observed in the study area. These structures show a strong relationship between the depth of faulting and the wavelength of the related anticlines, influencing the kinematics of the thrust system. The PT and CT structures are detached at depths of ~ 9 km on top of the acoustic basement. The two related PA and CA structures can be followed along strike for about 50 km and are characterized by a wavelength in the order of ~ 11 km. The TS develops along the shallow part of the Pesaro thrust at a depth of 3.5 km, is characterized by a short wavelength (~ 1.1 km) of the imbricates spread along ~ 5 km in the forelimb of PA, and it can be followed only for ~10 km along strike. The PT and CT en-echelon arrangement, the presence of multiple detachments and the thin-skinned deformation (multiple décollements) suggest a geological model for this outermost sector of the Apennines characterized by a thrust system not involving the acoustic basement (thin-skinned tectonics).

This study highlights a possible minor role of the Cornelia thrust system during the 2022 earthquakes than previously thought due to a more limited extent to the NW. Although based on its geological, structural and geometrical characteristics this thrust system cannot be excluded as a seismogenic source, the historical and recent seismicity directly affecting the CT, with its limited extension toward the north, is scarce and cannot be easily linked with it. The integration of the relocated hypocentres and the new geological model suggests that the PT, or a possible easternmost deeper structure, would be better candidates to be associated with the mainshocks. On the other hand, the relay zone between PT and CT is more coherent with the second main event. The still present uncertainty is mainly due to the low accuracy of the seismicity relocation caused by lack of seismic stations and simplified velocity models used. This work aims to remark that defining a solid subsurface geological model by integration of key reflection seismic profiles and boreholes data (even if legacy) is essential in offshore areas. Building up a reliable, geologically driven model, allows to refine not only velocity models to use for more accurate earthquakes' relocation, but for increasing the reliability of seismotectonic studies and risks assessments. The



advancement of geological and geophysical studies might have broader benefits also on other application, such as supporting safer exploration projects of carbon capture and storage along the **NA** sea region.

595 **Data availability**

Supplementary data associated with this article can be found, in the online version

Author contribution

ES, ME, and MB contributed to the conception and design of the study. ES performed data curation, analysis, investigation, methodology, visualization, preparation of tables, maps and figures, and wrote the original draft of the manuscript. ME
600 contributed to investigation, writing and revision. FC contributed to writing, revision, visualization maps and figures. FM and AA contributed to the investigation, and revision. MB was responsible for conceptualization, resources, supervision, and review and editing. All authors contributed to the final revision of the manuscript and approved the version submitted.

Competing interests

The authors declare that they have no conflict of interest

605

Acknowledgment:

The authors express their gratitude to Schlumberger, Cegal, and PE Limited for providing academic licenses for their software platforms and plugins to the University of Perugia. These software and tools were used for uploading scanned legacy seismic profiles and well data (Blueback tools, Cegal), well digitization, and seismic interpretation with Petrel, as
610 well as for structural modeling, and velocity model analysis with Petrel and Move. We also acknowledge the support teams of Petrel, Move, and Cegal for their prompt assistance in resolving technical challenges during the study. Additionally, we sincerely appreciate the QGIS and Inkscape Teams for developing free and open-source software, which was essential for data organization, correlation, and analysis (QGIS), as well as for image enhancement and digitization (Inkscape). We extend our special thanks to ENI for providing subsurface data under a confidential agreement, and to the Ministero dello
615 Sviluppo Economico DGRME, the Società Geologica Italiana, Assomineraria, and CNR ViDEPI (<https://www.arcgis.com/>) for granting access to public domain data and services. We are also grateful to An and the Pezzo groups for sharing with us their catalogs of the relocated seismicity.



References

- Alvarez, W., 1999. Drainage on evolving fold-thrust belts: a study of transverse canyons in the Apennines. *Basin Research* 11, 267–284.
- Amadori, C., Toscani, G., Di Giulio, A., Maesano, F.E., D'Ambrogi, C., Ghielmi, M. and Fantoni, R., 2019. From cylindrical to non-cylindrical foreland basin: Pliocene–Pleistocene evolution of the Po Plain–Northern Adriatic basin (Italy). *Basin Research*, 31(5), pp.991–1015. <https://doi.org/10.1111/bre.12369>.
- Amadori, C., Ghielmi, M., Mancin, N. and Toscani, G., 2020. The evolution of a coastal wedge in response to Plio-Pleistocene climate change: The Northern Adriatic case. *Marine and Petroleum Geology*, 122, p.104675. <https://doi.org/10.1016/j.marpetgeo.2020.104675>.
- An, L., Grigoli, F., Enescu, B., Buttinelli, M., Anselmi, M., Molinari, I. and Ito, Y., 2024. Offshore Fault Geometry Revealed from Earthquake Locations Using New State-of-Art Techniques: The Case of the 2022 Adriatic Sea Earthquake Sequence. *Seismological Research Letters*, 95(5), pp.2779–2790. <https://doi.org/10.1785/0220230264>.
- Argnani, A., 1998. Structural elements of the Adriatic foreland and their relationships with the front of the Apennine fold-and-thrust belt. *Memorie della Societa Geologica Italiana*, 52, 647–654.
- Bally, A.W., 1986. Balanced sections and seismic reflection profiles across the Central Apennines. *Mem. Soc. Geol. It.*, 35, pp.257–310.
- Barbieri, C., Di Giulio, A., Massari, F., Asioli, A., Bonato, M. and Mancin, N., 2007. Natural subsidence of the Venice area during the last 60 Myr. *Basin Research*, 19(1), pp.105–123. <https://doi.org/10.1111/j.1365-2117.2007.00314.x>
- Barchi M.R., De Feyter A., Magnani M.B., Minelli G., Piali G. & Sotera B.M. (1998) - The structural style of the Umbria-Marche fold and thrust belt. *Mem. Soc. Geol. It.* 52, 557–578.
- Barchi M.R., 2010. The Neogene-Quaternary evolution of the Northern Apennines: crustal structure, style of deformation and seismicity. In: (Eds.) Beltrando M., Peccerillo A., Mattei M., Conticelli S., and Doglioni C., *Journal of the Virtual Explorer*, volume 36, paper 10, doi: 10.3809/jvirtex.2009.00220.
- Barchi, M.R., Alvarez, W. and Shimabukuro, D.H., 2012. The Umbria-Marche Apennines as a double orogen: observations and hypotheses. *Italian Journal of Geosciences*, 131(2), pp.258–271. <https://doi.org/10.3301/IJG.2012.17>
- Barchi, M.R., Carboni, F., Michele, M., Ercoli, M., Giorgetti, C., Porreca, M., Azzaro, S. and Chiaraluca, L., 2021. The influence of subsurface geology on the distribution of earthquakes during the 2016–2017 Central Italy seismic sequence. *Tectonophysics*, 807, p.228797. <https://doi.org/10.1016/j.tecto.2021.228797>
- Berberian, M., 1995. Master “blind” thrust faults hidden under the Zagros folds: active basement tectonics and surface morphotectonics. *Tectonophysics* 241, 193–224. [https://doi.org/10.1016/0040-1951\(94\)00185-C](https://doi.org/10.1016/0040-1951(94)00185-C)
- Bigi, G., Cosentino, D., Parotto, M., Sartori, R., & Scandone, P., 1992. Structural model of Italy and gravity map, 1:500,000. S.EL.CA.
- Bianco, E., 2014. Geophysical tutorial: Well-tie calculus. *The Leading Edge*, 33(6), pp.674–677.



- Billi, A., 2005. Attributes and influence on fluid flow of fractures in foreland carbonates of southern Italy. *Journal of Structural Geology*, 27, 1630-1643.
- Brancolini, G., Civile, D., Donda, F., Tosi, L., Zecchin, M., Volpi, V., Rossi, G., Sandron, D., Ferrante, G.M., Forlin, E., 2019. New insights on the Adria plate geodynamics from the northern Adriatic perspective. *Mar. Petrol. Geol.* 109, 687–697.
- 655 Bonini, L., Toscani, G. and Seno, S., 2014. Three-dimensional segmentation and different rupture behavior during the 2012 Emilia seismic sequence (Northern Italy). *Tectonophysics*, 630, pp.33-42.
- Boschi E., Guidoboni E., Ferrari G., Mariotti D., Valensise G., Gasperini P. (eds), 2000. Catalogue of Strong Italian Earthquakes from 461 B.C. to 1997. *Annali di Geofisica*, 43, 4, 609-868.
- Burrato, P., Vannoli, P., Fracassi, U., Basili, R. and Valensise, G., 2012. Is blind faulting truly invisible? Tectonic-controlled
660 drainage evolution in the epicentral area of the May 2012, Emilia-Romagna earthquake sequence (northern Italy). *Annals of Geophysics*.
- Carboni, F., Brozzetti, F., Mirabella, F., Cruciani, F., Porreca, M., Ercoli, M., Back, S., Barchi, M.R., 2020a. Geological and geophysical study of a thin-skinned tectonic wedge formed during an early collisional stage: the Trasimeno Tectonic Wedge (Northern Apennines, Italy). *Geol. Mag.* 157 (2), 213–232. <https://doi.org/10.1017/S001675681900061X>.
- 665 Carboni, F., Viola, G., Aldega, L., Van der Leij, R., Brozzetti, F., Barchi, M.R., 2020b. K-Ar fault gouge dating of Neogene thrusting: the case of the siliciclastic deposits of the Trasimeno Tectonic Wedge (Northern Apennines, Italy). *Ital. J. Geosci.* 139 (2), 300–308. <https://doi.org/10.3301/IJG.2020.06>.
- Carboni, F., Mirabella, F., Minelli, G., Saleh, H., Porreca, M., Ercoli, M., Pauselli, C. and Barchi, M.R., 2024. Kinematic reconstruction of active tectonic and halokinetic structures in the 2021 NW Palagruža earthquake area (Central Adriatic).
670 *Journal of Structural Geology*, 182, p.105112.
- Caricchi, C., Cifelli, F., Sagnotti, L., Sani, F., Speranza, F. and Mattei, M., 2014. Paleomagnetic evidence for a post-Eocene 90° CCW rotation of internal Apennine units: A linkage with Corsica-Sardinia rotation. *Tectonics*, 33(4), pp.374-392.
- Carminati, E., Corda, L., Mariotti, G., Scifoni, A. and Trippetta, F., 2013. Mesozoic syn-and postdrift evolution of the central Apennines, Italy: the role of triassic evaporites. *The Journal of Geology*, 121(4), pp.327-354.
- 675 Casero, P. and Bigi, S., 2013. Structural setting of the Adriatic basin and the main related petroleum exploration plays. *Marine and Petroleum Geology*, 42, pp.135-147.
- Castellarin, A., Eva, C., Giglia, G., Vai, G.B., Rabbi, E., Pini, G.A. and Crestana, G., 1985. Analisi strutturale del fronte appenninico padano. *Giornale di Geologia*, 47(1-2), pp.47-75.
- Centamore, E., Adamoli, L., Berti, D., Bigi, G., Bigi, S., Casnedi, R., Cantalamessa, G., Fumanti, F., Morelli, C., Micarelli, A. and Ridolfi, M., 1992. Carta geologica dei bacini della Lagaffe del Cellino e dei rilievi carbonatici circostanti. *Studi Geologici Camerti*, Vol. Spec.
- 680 Channell, J.E., d'Argenio, B. and Horvath, F., 1979. Adria, the African promontory, in *Mesozoic Mediterranean palaeogeography*. *Earth-Science Reviews*, 15(3), pp.213-292.



- Chiaraluce, L., Barchi, M.R., Carannante, S., Collettini, C., Mirabella, F., Pauselli, C. and Valoroso, L., 2017. The role of
 685 rheology, crustal structures and lithology in the seismicity distribution of the northern Apennines. *Tectonophysics*, 694,
 pp.280-291.
- Ciaccio, M.G., Barchi, M.R., Chiarabba, C., Mirabella, F. and Stucchi, E., 2005. Seismological, geological and geophysical
 constraints for the Gualdo Tadino fault, Umbria–Marche Apennines (central Italy). *Tectonophysics*, 406(3-4), pp.233-247.
- Costanzo, A., 2024. A New Catalogue and Insights into the 2022 Adriatic Offshore Seismic Sequence Using a Machine
 690 Learning-Based Procedure. *Sensors*, 25(1), p.82.
- Cuffaro, M., Riguzzi, F., Scrocca, D., Antonioli, F., Carminati, E., Livani, M. and Doglioni, C., 2010. On the geodynamics
 of the northern Adriatic plate. *Rendiconti Lincei*, 21, pp.253-279.
- Dahlstrom, C.D., 1970. Structural geology in the eastern margin of the Canadian Rocky Mountains. *Bulletin of Canadian
 Petroleum Geology*, 18(3), pp.332-406.
- 695 D'agostino, N., Avallone, A., Cheloni, D., D'anastasio, E., Mantenuto, S. and Selvaggi, G., 2008. Active tectonics of the
 Adriatic region from GPS and earthquake slip vectors. *Journal of Geophysical Research: Solid Earth*, 113(B12).
- De Feyter, A.J., Koopman, A., Molenaar, N., Ende, C.V.D., 1986. Detachment tectonics and sedimentation, Umbro-
 Marchean Apennines, (Italy). *Bollettino della Società Geologica Italiana* 105, 65–85.
- De Feyter, A.J., 1991. *Gravity tectonics and sedimentation of the Montefeltro, Italy* (No. 35). Faculteit Aardwetenschappen
 700 der Rijksuniversiteit te Utrecht.
- De Nardis, R., Pandolfi, C., Cattaneo, M., Monachesi, G., Cirillo, D., Ferrarini, F., Bello, S., Brozzetti, F. and Lavecchia, G.,
 2022. Lithospheric double shear zone unveiled by microseismicity in a region of slow deformation. *Scientific Reports*, 12(1),
 p.21066.
- Déverchère, J., Yelles, K., Domzig, A., Mercier de Lépinay, B., Bouillin, J.P., Gaullier, V., Bracène, R., Calais, E., Savoye,
 705 B., Kherroubi, A. and Le Roy, P., 2005. Active thrust faulting offshore Boumerdes, Algeria, and its relations to the 2003 Mw
 6.9 earthquake. *Geophysical research letters*, 32(4).
- Dewey, J.F., Helman, M.L., Knott, S.D., Turco, E. and Hutton, D.H.W., 1989. Kinematics of the western Mediterranean.
Geological Society, London, Special Publications, 45(1), pp.265-283.
- Di Bucci, D., Mazzoli, S., 2002. Active tectonics of the Northern Apennines and Adria geodynamics: new data and a
 710 discussion. *Journal of Geodynamics*, 34, Issue 5, 687-707. [https://doi.org/10.1016/S0264-3707\(02\)00107-2](https://doi.org/10.1016/S0264-3707(02)00107-2).
- DISS Working Group (2021). Database of Individual Seismogenic Sources (DISS), Version 3.3.0: A compilation of
 potential sources for earthquakes larger than M 5.5 in Italy and surrounding areas. Istituto Nazionale di Geofisica e
 Vulcanologia (INGV). <https://doi.org/10.13127/diss3.3.0>.
- Ercoli, M., Carboni, F., Akimbekova, A., Carbonell, R.B. and Barchi, M.R., 2023. Evidencing subtle faults in deep seismic
 715 reflection profiles: Data pre-conditioning and seismic attribute analysis of the legacy CROP-04 profile. *Frontiers in Earth
 Science*, 11, p.1119554.



- Fantoni, R. & Franciosi, R., 2010. Tectono-sedimentary setting of the Po Plain and Adriatic foreland. *Rendiconti Lincei*, 21, 197–209.
- Finetti, I.R., Del Ben, A., 2005. Crustal Tectono-Stratigraphic Setting of the Adriatic Sea from New CROP Seismic Data. *CROP PROJECT: Deep*. Elsevier, pp. 519–547 (Chapter 23)
- Franklin D. Wolfe, John H. Shaw, Andreas Plesch, Daniel J. Ponti, James F. Dolan, Mark R. Legg; The Wilmington Blind-Thrust Fault: An Active Concealed Earthquake Source beneath Los Angeles, California. *Bulletin of the Seismological Society of America* 2019; 109 (5): 1890–1906. doi: <https://doi.org/10.1785/0120180335>.
- Frignani, M. and Langone, L., 1991. Accumulation rates and ¹³⁷Cs distribution in sediments off the Po River delta and the Emilia-Romagna coast (northwestern Adriatic Sea, Italy). *Continental Shelf Research*, 11(6), pp.525–542.
- Geletti, R., Del Ben, A., Busetti, M., Ramella, R. and Volpi, V. (2008), Gas seeps linked to salt structures in the Central Adriatic Sea. *Basin Research*, 20: 473–487. <https://doi.org/10.1111/j.1365-2117.2008.00373.x>.
- Ghielmi, M., Minervini, M., Nini, C., Rogledi, S., Rossi, M., 2010a. Sedimentary and tectonic evolution in the eastern Po Plain and northern Adriatic Sea area from Messinian to Middle Pleistocene (Italy). In: Sassi, F.P. (Ed.), *Nature and Geodynamics of the Lithosphere in Northern Adriatic*. *Rend. Fis. Acc. Lincei*, 21 (Suppl.1), pp. 131–166. <http://dx.doi.org/10.1007/s12210-010-0101-5>.
- Ghielmi, M., Minervini, M., Nini, C., Rogledi, S. and Rossi, M., 2013. Late Miocene–Middle Pleistocene sequences in the Po Plain–Northern Adriatic Sea (Italy): the stratigraphic record of modification phases affecting a complex foreland basin. *Marine and Petroleum Geology*, 42, pp.50–81.
- Guidoboni, E., Ferrari, G., Tarabusi, G., Sgattori, G., Comastri, A., Mariotti, D., Ciuccarelli, C., Bianchi, M.G. and Valentini, G., 2019. CFTI5Med, the new release of the catalogue of strong earthquakes in Italy and in the Mediterranean area. *Scientific Data*, 6(1), p.80.
- Gunderson, K. L., Anastasio, D. J., Pazzaglia, F. J., and Picotti, V. (2013). Fault slip rate variability on 104–105yr timescales for the Salsomaggiore blind thrust fault, Northern Apennines, Italy. *Tectonophysics* 608, 356–365. doi: 10.1016/j.tecto.2013.09.018.
- Gunderson, K.L., Anastasio, D.J., Pazzaglia, F.J. and Kodama, K.P., 2018. Intrinsically variable blind thrust faulting. *Tectonics*, 37(5), pp.1454–1471
- Handy, M. R., Ustaszewski, K., & Kissling, E., 2015. Reconstructing the Alps–Carpathians–Dinarides as a key to understanding switches in subduction polarity, slab gaps and surface motion. *International Journal of Earth Sciences*, 104(1), 1–26. <https://doi.org/10.1007/s00531-014-1060-3>.
- Hayes, G.P., Briggs, R.W., Sladen, A., Fielding, E.J., Prentice, C., Hudnut, K., Mann, P., Taylor, F.W., Crone, A.J., Gold, R. and Ito, T., 2010. Complex rupture during the 12 January 2010 Haiti earthquake. *Nature Geoscience*, 3(11), pp.800–805.
- Van Hinsbergen, D.J., Torsvik, T.H., Schmid, S.M., Matenco, L.C., Maffione, M., Vissers, R.L., Gürer, D. and Spakman, W., 2020. Orogenic architecture of the Mediterranean region and kinematic reconstruction of its tectonic evolution since the Triassic. *Gondwana Research*, 81, pp.79–229.



- Koopman, A., 1983. Detachment tectonics in the central Apennines, Italy (Doctoral dissertation, Instituut voor Aardwetenschappen der Rijksuniversiteit te Utrecht).
- Latorre, D., Mirabella, F., Chiaraluce, L., Trippetta, F. and Lomax, A., 2016. Assessment of earthquake locations in 3-D deterministic velocity models: A case study from the Altotiberina Near Fault Observatory (Italy). *Journal of Geophysical Research: Solid Earth*, 121(11), pp.8113-8135.
- Lavecchia, G., 1981. Appunti per uno schema strutturale dell'Appennino Umbro-Marchigiano. III: Lo stile deformativo.
- Lavecchia, G., Minelli, G. and Pialli, G., 1988. The Umbria-Marche arcuate fold belt (Italy). *Tectonophysics*, 146(1-4), pp.125-137.
- Lavecchia, G., Boncio, P., Creati, N., Brozzetti, F., 2004. Stile strutturale, stato termico-meccanico e significato sismogenetico del thrust Adriatico: dati e spunti da una revisione del profilo CROP 03 integrata con l'analisi di dati sismologici. *Bollettino della Societa` Geologica Italiana* 123, 111–125.
- Lavecchia, G., Pietrolungo, F., Bello, S., Talone, D., Pandolfi, C., Andrenacci, C., Carducci, A. and de Nardis, R., 2023. Slowly Deforming Megathrusts within the Continental Lithosphere: A Case from Italy. *GSA TODAY*, 34(1), pp.4-10.
- Leonard, M., 2014. Self-consistent earthquake fault-scaling relations: Update and extension to stable continental strike-slip faults. *Bulletin of the Seismological Society of America*, 104(6), pp.2953-2965.
- Lettis, W.R., Wells, D.L. and Baldwin, J.N., 1997. Empirical observations regarding reverse earthquakes, blind thrust faults, and quaternary deformation: Are blind-thrust faults truly blind? *Bulletin of the Seismological Society of America*, 87(5), pp.1171-1198.
- Livani, M., Scrocca, D., Arecco, P. and Doglioni, C., 2018. Structural and stratigraphic control on salient and recess development along a thrust belt front: The Northern Apennines (Po Plain, Italy). *Journal of Geophysical Research: Solid Earth*, 123(5), pp.4360-4387.
- Locati M., Camassi R., Rovida A., Ercolani E., Bernardini F., Castelli V., Caracciolo C.H., Tertulliani A., Rossi A., Azzaro R., D'Amico S., Antonucci A., 2022. Database Macrosismico Italiano (DBMI15), versione 4.0 [Data set]. Istituto Nazionale di Geofisica e Vulcanologia (INGV). <https://doi.org/10.13127/dbmi/dbmi15.4>
- Ioualalen, Bernard Pelletier, Gabriela Solis Gordillo, Investigating the March 28th 1875 and the September 20th 1920 earthquakes/tsunamis of the Southern Vanuatu arc, offshore Loyalty Islands, New Caledonia, *Tectonophysics*, Volume 709, 2017, Pages 20-38, ISSN 0040-1951, <https://doi.org/10.1016/j.tecto.2017.05.006>
- Maesano, F. E., Toscani, G., Burrato, P., Mirabella, F., D'Ambrogio, C., and Basili, R., 2013. Deriving thrust fault slip rates from geological modeling: Examples from the Marche coastal and offshore contraction belt, Northern Apennines, Italy. *Mar. Petrol. Geol.* 42, 122–134. doi: 10.1016/j.marpetgeo.2012.10.008.
- Maesano, F. E., D'Ambrogio, C., Burrato, P., & Toscani, G., 2015. Slip-rates of blind thrusts in slow deforming areas: examples from the Po Plain (Italy). *Tectonophysics*, 643, 8-25.
- Latorre, D., Mirabella, F., Chiaraluce, L., Trippetta, F., Lomax, A., 2016. Assessment of earthquake locations in 3-D deterministic velocity models: A case study from the Altotiberina Near Fault Observatory (Italy): Event Locations in



- 785 Deterministic Models. *Journal of Geophysical Research: Solid Earth* 121, 8113–8135.
<https://doi.org/10.1002/2016JB013170>
- Maesano, F. E., & D'Ambrogi, C., 2016. Coupling sedimentation and tectonic control: Pleistocene evolution of the central Po Basin. *Italian Journal of Geosciences*, 135(3), 394-407.
- Maesano, F. E., Buttinelli, M., Maffucci, R., Toscani, G., Basili, R., Bonini, L., et al., 2023. Buried alive: Imaging the 9
 790 November 2022, Mw 5.5 earthquake source on the offshore Adriatic blind thrust front of the Northern Apennines (Italy).
Geophysical Research Letters, 50, e2022GL102299. <https://doi.org/10.1029/2022GL102299>.
- Mantovani, E., Babbucci, D., Viti, M., Albarello, D., Mugnaioli, E., Cenni, N., et al., 2006. Post-Late Miocene kinematics of the Adria microplate: inferences from geological, geophysical and geodetic data, in *The Adria Microplate: GPS Geodesy, Tectonics and Hazards. Nato Science Series: IV: Earth and Environmental Sciences*, 61, 51–69. doi: 10.1007/1-4020-4235-
 795 3_04.
- Maramai, A., Brizuela, B. and Graziani, L., 2022. A Database for Tsunamis and Meteotsunamis in the Adriatic Sea. *Applied Sciences*, 12(11), p.5577.
- Massoli, D., Koyi, H.A. and Barchi, M.R., 2006. Structural evolution of a fold and thrust belt generated by multiple décollements: analogue models and natural examples from the Northern Apennines (Italy). *Journal of Structural Geology*,
 800 28(2), pp.185-199.
- Mattavelli, L., Novelli, L. & Anelli, L., 1991. Occurrence of hydrocarbons in the Adriatic basin. *Spec. Publ. EAPG*, 1, 369-380.
- Mazzanti, R. and Trevisan, L., 1978. Evoluzione della rete idrografica nell'Appennino centro-settentrionale. *Geografia Fisica e Dinamica Quaternaria*, 1(1), pp.55-62.
- 805 Mazzoli, S., Santini, S., Macchiavelli, C., & Ascione, A., 2015. Active tectonics of the outer northern Apennines: Adriatic vs. Po Plain seismicity and stress fields. *Journal of Geodynamics*, 84, 62–76.
<https://doi.org/10.1016/j.jog.2014.10northern.002>.
- Menichetti, M. and Coccioni, R., 2013. Umbria-Marche Apennines geological field trip.
- Mirabella, F., Ciaccio M.G., Barchi M.R., Merlini S., 2004. The Gubbio normal fault (Central Italy): geometry, displacement
 810 distribution and tectonic evolution, *Journal of Structural Geology*. 26, 2233-2249, ISSN 0191-8141,
<https://doi.org/10.1016/j.jsg.2004.06.009>.
- Mirabella, F., Barchi, M. R., & Lupattelli, A., 2008. Seismic reflection data in the Umbria Marche region: Limits and capabilities to unravel the subsurface structure in a seismically active area. *Annals of Geophysics*, 51(2–3), 383–396.
<https://doi.org/10.4401/ag-3032>.
- 815 Molli, G., 2008. Northern Apennine–Corsica orogenic system: an updated overview (Vol. 298, No. 1, pp. 413-442). London: The Geological Society of London.
- Molli, G. and Malavieille, J., 2011. Introduction to the Field trips of the CorseAlp 2011. *Journal of the Virtual Explorer*, 39, pp.paper-1.



- Montone, P. and Mariucci, M.T., 2023. Deep well new data in the area of the 2022 Mw 5.5 earthquake, Adriatic Sea, Italy: In situ stress state and P-velocities. *Frontiers in Earth Science*, 11, p.1164929.
- Nespoli, M., Belardinelli, M.E., Gualandi, A., Serpelloni, E. and Bonafede, M., 2018. Poroelasticity and fluid flow modeling for the 2012 Emilia-Romagna earthquakes: Hints from GPS and InSAR data. *Geofluids*, 2018(1), p.4160570.
- Ollier, C.D. and Pain, C.F., 2009. The Apennines, the Dinarides, and the Adriatic Sea: is the Adriatic Microplate a reality?. *Geografia Fisica e Dinamica Quaternaria*, 32(2), pp.167-175.
- Palano, M., Pezzo, G., Serpelloni, E., Devoti, R., D'Agostino, N., Gandolfi, S., Sparacino, F., Anderlini, L., Poluzzi, L., Tavasci, L. and Macini, P., 2020. Geopositioning time series from offshore platforms in the Adriatic Sea. *Scientific Data*, 7(1), p.373.
- Panara Y, Maesano FE, Amadori C, Fedorik J, Toscani G and Basili R., 2021. Probabilistic Assessment of Slip Rates and Their Variability Over Time of Offshore Buried Thrusts: A Case Study in the Northern Adriatic Sea. *Front. Earth Sci.* 9:664288. doi: 10.3389/feart.2021.664288.
- Pandolfi, C., Taroni, M., de Nardis, R., Lavecchia, G. and Akinci, A., 2024. Advanced 3D seismic hazard analysis for active compression in the Adriatic Thrust Zone, Italy. *Bulletin of Earthquake Engineering*, pp.1-24.
- Pauselli, C., Marchesi, R. and Barchi, M.R., 2002. Seismic image of the compressional and extensional structures in the Gubbio area (Umbrian-Pre Apennines). *BOLLETTINO DELLA SOCIETÀ GEOLOGICA ITALIANA. VOLUME SPECIALE*, pp.263-272.
- Pauselli, C., Barchi, M.R., Federico, C., Magnani, M.B. and Minelli, G., 2006. The crustal structure of the Northern Apennines (Central Italy): an insight by the CROP03 seismic line. *American Journal of Science*, 306(6), pp.428-450.
- Pezzo, G., Merryman Boncori, J.P., Tolomei, C., Salvi, S., Atzori, S., Antonioli, A., Trasatti, E., Novali, F., Serpelloni, E., Candela, L. and Giuliani, R., 2013. Coseismic deformation and source modeling of the May 2012 Emilia (Northern Italy) earthquakes. *Seismological Research Letters*, 84(4), pp.645-655.
- Pezzo, G., Petracchini, L., Devoti, R., Maffucci, R., Anderlini, L., Antoncicchi, I., et al., 2020. Active fold-thrust belt to foreland transition in northern Adria, Italy, tracked by seismic reflection profiles and GPS offshore data. *Tectonics*, 39, e2020TC006425. <https://doi.org/10.1029/2020TC006425> Received 9 JUL 2020 Accepted 7 OCT 2020 Accepted article online 9 NOV 2020 PEZZO ET AL. 1 of 21
- Pezzo, G., Billi, A., Carminati, E. et al., 2023. Seismic source identification of the 9 November 2022 Mw 5.5 offshore Adriatic Sea (Italy) earthquake from GNSS data and aftershock relocation. *Sci Rep* 13, 11474. <https://doi.org/10.1038/s41598-023-38150-5>.
- Piccardi, L., Sani, F., Moratti, G., Cunningham, D. and Vittori, E., 2011. Present-day geodynamics of the circum-Adriatic region: An overview. *Journal of geodynamics*, 51(2-3), pp.81-89.
- Pieri, M. and Groppi, G., 1981. Subsurface geological structure of the Po Plain, Italy. Verlag nicht ermittelbar.



- Porreca, M., Minelli, G., Ercoli, M., Brobia, A., Mancinelli, P., Cruciani, F., et al (2018). Seismic reflection profiles and subsurface geology of the area interested by the 2016–2017 earthquake sequence (Central Italy). *Tectonics*, 37, 1116–1137. <https://doi.org/10.1002/2017TC004915>.
- Ricci Lucchi, F., 1986. The Oligocene to Recent foreland basins of the northern Apennines. *Foreland basins*, pp.103-139.
- 855 Roering, J., Cooke, M.L., Pollard, D., 1997. Why blind thrust faults do not propagate to the Earth's surface: numerical modeling of coseismic deformation associated with thrust-related anticlines. *J. Geophys. Res.* 102, 11901–11912.
- Rovida, A., Locati, M., Camassi, R., Lolli, B., Gasperini, P., & Antonucci, A. (2022). Catalogo Parametrico dei Terremoti Italiani (CPTI15), versione 4.0 [Dataset]. Istituto Nazionale di Geofisica e Vulcanologia (INGV). <https://doi.org/10.13127/CPTI/CPTI15.4>.
- 860 Sani, F., Vannucci, G., Boccaletti, M., Bonini, M., Corti, G. and Serpelloni, E., 2016. Insights into the fragmentation of the Adria Plate. *Journal of Geodynamics*, 102, pp.121-138.
- Scarsella, F. (1941). Carta geologica d'Italia, foglio 132, Norcia. Roma: Regio Ufficio Geologico.
- Schmid, S.M., Fügenschuh, B., Kissling, E. and Schuster, R., 2004. Tectonic map and overall architecture of the Alpine orogen. *Eclogae Geologicae Helveticae*, 97, pp.93-117.
- 865 Schmid, S.M., Fügenschuh, B., Kounov, A., Maţenco, L., Nievergelt, P., Oberhänsli, R., Pleuger, J., Schefer, S., Schuster, R., Tomljenović, B. and Ustaszewski, K., 2020. Tectonic units of the Alpine collision zone between Eastern Alps and western Turkey. *Gondwana Research*, 78, pp.308-374.
- Scholz, C.H., 2019. *The mechanics of earthquakes and faulting*. Cambridge university press.
- Scisciani, V., Esetime, P., 2017. The Triassic evaporites in the evolution of the Adriatic Basin. In: Soto, J.I., Flinch, J.F., Tari, G. (Eds.), *Permo-Triassic salt provinces of Europe, North Africa, and Atlantic margins: Tectonics and Hydrocarbon Potential*. Elsevier, Amsterdam, 499-516.
- 870 Scognamiglio, L., Margheriti, L., Mele, F.M., Tinti, E., Bono, A., De Gori, P., Lauciani, V., Lucente, F.P., Mandiello, A.G., Marocci, C. and Mazza, S., 2012. The 2012 Pianura Padana Emiliana seismic sequence: locations, moment tensors and magnitudes. *Annals Geophysics*.
- 875 Sorlien, C.C., Seeber, L., Broderick, K.G., Luyendyk, B.P., Fisher, M.A., Sliter, R.W. and Normark, W.R., 2013. The Palos Verdes anticlinorium along the Los Angeles, California coast: Implications for underlying thrust faulting. *Geochemistry, Geophysics, Geosystems*, 14(6), pp.1866-1890.
- Stampfli, G.M. and Borel, G.D., 2002. A plate tectonic model for the Paleozoic and Mesozoic constrained by dynamic plate boundaries and restored synthetic oceanic isochrons. *Earth and Planetary science letters*, 196(1-2), pp.17-33.
- 880 Sugan, M., Campanella, S., Chiaraluce, L., Michele, M., & Vuan, A., 2023. The unlocking process leading to the 2016 Central Italy seismic sequence. *Geophysical Research Letters*, 50, e2022GL101838. <https://doi.org/10.1029/2022GL101838> Received 21 OCT 2022 Accepted 12 JAN 2023 10.1029/2022GL101838.
- Takashimizu, Y., Kawakami, G. and Urabe, A., 2020. Tsunamis caused by offshore active faults and their deposits. *Earth-Science Reviews*, 211, p.103380.



- 885 Tavarnelli, E., 1997. Structural evolution of a foreland fold-and-thrust belt: the Umbria-Marche Apennines, Italy. *Journal of Structural Geology*, 19(3-4), pp.523-534.
- Tavarnelli, E., Scisciani, V., Patruno, S., Calamita, F., Pace, P. and Iacopini, D., 2019. The role of structural inheritance in the evolution of fold-and-thrust belts: insights from the Umbria-Marche Apennines, Italy.
- Tertulliani, A., Arcoraci, L., Berardi, M., Bernardini, F., Brizuela, B., Castellano, C., Ercolani, E., Graziani, L., Maramai, A.,
- 890 Rossi, A. and Sbarra, M., 2012. The Emilia 2012 sequence: a macroseismic survey. *Annals of Geophysics*.
- Tinterri, R., Lipparini, L., 2013. Seismo-stratigraphic study of the Plio-Pleistocene foredeep deposits of the Central Adriatic Sea (Italy): geometry and characteristics of deep-water channels and sediment waves. *Mar. Petrol. Geol.*, 42, 30-49.
- Tizzani, P., Castaldo, R., Solaro, G., Pepe, S., Bonano, M., Casu, F., Manunta, M., Manzo, M., Pepe, A., Samsonov, S. and Lanari, R., 2013. New insights into the 2012 Emilia (Italy) seismic sequence through advanced numerical modeling of ground
- 895 deformation InSAR measurements. *Geophysical research letters*, 40(10), pp.1971-1977.
- Tizzani, P., Castaldo, R., Solaro, G., Pepe, S., Bonano, M., Casu, F., Manunta, M., Manzo, M., Pepe, A., Samsonov, S. and Lanari, R., 2013. New insights into the 2012 Emilia (Italy) seismic sequence through advanced numerical modeling of ground deformation InSAR measurements. *Geophysical research letters*, 40(10), pp.1971-1977.
- Ustaszewski, K., Kounov, A., Schmid, S.M., Schaltegger, U., Krenn, E., Frank, W. and Fügenschuh, B., 2010. Evolution of
- 900 the Adria-Europe plate boundary in the northern Dinarides: From continent-continent collision to back-arc extension. *Tectonics*, 29(6).
- van Unen, M., Matenco, L., Nader, F.H., Darnault, R., Mandic, O. and Demir, V., 2019. Kinematics of foreland-vergent crustal accretion: Inferences from the Dinarides evolution. *Tectonics*, 38(1), pp.49-76.
- Vannoli, P., Burrato, P. and Valensise, G., 2015. The seismotectonics of the Po Plain (northern Italy): Tectonic diversity in a
- 905 blind faulting domain. *Pure and Applied Geophysics*, 172, pp.1105-1142.
- Wells, D.L. and Coppersmith, K.J., 1994. New empirical relationships among magnitude, rupture length, rupture width, rupture area, and surface displacement. *Bulletin of the seismological Society of America*, 84(4), pp.974-1002.
- Wrigley, R., Hodgson, N., Esetime, P., 2015. Petroleum geology and hydrocarbon potential of the Adriatic basin, offshore Croatia. *J. Petrol. Geol.* 38 (3), 301–316.
- 910 **Web references**
- <https://diss.ingv.it/>
- <https://www.terremoti.ingv.it>
- <https://www.videpi.com>